Woodgate, M. A., Pastrikakis, V. A., and Barakos, G. N. (2016) Method for calculating rotors with active gurney flaps. Journal of Aircraft, 53(3), pp. 605-626.

There may be differences between this version and the published version. You are advised to consult the publisher's version if you wish to cite from it.

http://eprints.gla.ac.uk/116464/

Deposited on: 15 July 2016

A Method for Calculating Rotors with Active Gurney Flaps

M. A. Woodgate,[*] V. A. Pastrikakis,[†] and G. N. Barakos[‡]

CFD Laboratory, School of Engineering, University of Liverpool

Liverpool L63 3GH, United Kingdom

This paper builds on the Helicopter Multi-Block version 2 CFD solver of the University of Liverpool and demonstrates the implementation and use of Gurney flaps on wings, and rotors. The idea is to flag any cell face within the computational mesh with a solid, no slip boundary condition. Hence the infinitely thin Gurney can be approximated by "blocking cells" in the mesh. Comparison between thick Gurney flaps and infinitely thin Gurneys showed no difference on the integrated loads, the same flow structure was captured and the same vortices were identified ahead and behind the Gurney. The results presented for various test cases suggest that the method is simple and efficient and it can therefore be used for routine analysis of rotors with Gurney flaps. Moreover, the current method adds to the flexibility of the solver since no special grids are required and Gurney flaps can be easily implemented. Simple 2D aerofoil, 3D wing, and rotors in hover and forward flight were tested with fixed, linearly actuated, and swinging Gurneys, and the ability of the code to deploy a Gurney flap within the multiblock mesh is highlighted. The need for experimental data suitable for validation of CFD methods for cases of rotors with Gurney flaps is also highlighted.

[*]AgustaWestland Fellow, CFD Laboratory, Department of Engineering, email: woodgate@liv.ac.uk
[†]Ph.D. Candidate, CFD Laboratory, Department of Engineering, email: vasileios.pastrikakis@liverpool.ac.uk
[‡]Professor, CFD Laboratory, Department of Engineering, email: g.barakos@liv.ac.uk, Corresponding author.

Notation

GREEK

α	$=$	Lift slope
β	$=$	Flapping angle at 75%R
θ	$=$	Blade pitch angle at 75%R
β_c, β_s	$=$	Flap harmonics
θ_c, θ_s	$=$	Pitch harmonics
β_0	$=$	Mean flapping angle at 75%R
θ_0	$=$	Mean pitch angle at 75%R
μ	$=$	Advance ratio
ρ	$=$	Density, kg/m^3
ΔA	$=$	Fraction of the area covered by the Gurney flap over the area of the cell face

LATIN

Re	$=$	Reynolds Number
M	$=$	Mach number
A_{gurney}	$=$	Area that the Gurney flap covers
C_L	$=$	Lift coefficient
C_D	$=$	Drag coefficient
C_M	$=$	Moment coefficient
C_P	$=$	Pressure coefficient
F_Z	$=$	Normal force
F_Y	$=$	In-plane force
L_z	$=$	Rotor loading along the span in the thrust direction
L_m	$=$	Rotor moment loading around the blade pitch axis
L_q	$=$	Rotor moment loading around the shaft axis
C_T	$=$	Thrust coefficient, $C_T = \frac{T}{\frac{1}{2}\rho\pi R^2 V_{tip}^2}$
C_Q	$=$	Torque coefficient, $C_Q = \frac{Q}{\frac{1}{2}\rho\pi R^3 V_{tip}^2}$
C_t	$=$	Sectional thrust coefficient, $C_t = \frac{L_z}{\frac{1}{2}\rho c V_{tip}^2}$
C_m	$=$	Sectional moment coefficient, $C_m = \frac{L_m}{\frac{1}{2}\rho c^2 V_{tip}^2}$
C_q	$=$	Sectional torque coefficient, $C_q = \frac{L_q}{\frac{1}{2}\rho c^2 V_{tip}^2}$

LATIN

U	=	Velocity component in x-direction
V	=	Velocity component in y-direction
BVI	=	Blade Vortex Interaction
R	=	Radius in chords
c	=	Blade mean chord
CFD	=	Computational Fluid Dynamics
RANS	=	Reynolds Averaged Navier-Stokes
URANS	=	Unsteady RANS

Subscripts

∞	=	Free-stream Value
tip	=	Tip value

I. Introduction

The use of Gurney flaps for lift enhancement is well established in the aerospace community and several research works document the advantages and limitations of these devices [1]. The best know application is in medium Reynolds number flows of racing cars. In its simplest form it is a small vertical strip a few percent of the chord of the aerofoil, attached to the trailing edge of the wing. The Gurney flap was first studied by Liebeck [2] and was followed up by numerous experimental studies [3–5]. Tang and Dowell [6] compared the experimental loading of a NACA0012 with both static and an oscillating trailing-edge Gurney flaps using an incompressible Navier-Stokes solver. Due to the scarcity of experimental data for dynamically deployed Gurney flaps, most computational studies to date have been conducted for that case [7–9]. Camocardi *et al.* [10] studied movable Gurney flaps on a NACA 4412 aerofoil to determine the flow pattern characteristics downstream the aerofoil in the near wake and they observed that the frequency that a Gurney flap oscillates outside and inside the aerofoil can promote an increase or a decrease of the total lift. Lee [11] also studied the impact of Gurney flaps of different heights and perforations on the growth and development of the tip vortex generated by a NACA 0012 wing using particle image velocimetry. The peak vorticity of the tip vortex found to be increased with bigger flap height, while the flap perforation led to both lift and drag coefficient decrease. Overall the lift-to-drag ratio was improved compared to the case with a solid flap of the same height. Recently, Cole *et al.* [12] studied the effect of Gurney flaps of different heights and chordwise locations to five aerofoils using a low-speed, low-turbulence wind tunnel. The results highlighted the fact that the aerofoil shape determines the aerodynamic performance of the aerofoil employing a Gurney flap.

In recent years, researchers returned to Gurney flaps to examine possible benefits on rotors [13, 14]. As an example, Min *et al.* [15] studied the effects of Gurney flaps on the blade root loads and hub vibratory loads. In their study, a Gurney flap was deployed over the entire span of the blade. Finally, Palacios *et al.* [16] compared both experimentally and numerically the power required to deploy a Gurney flap against a plain flap on a K-max rotor blade, as well as the efficiency of those devices. According to the authors, Gurney flaps appear to be most suitable where the devices can enable improved reliability or the deployment mechanisms heavily favour Gurney flaps over plain flaps.

The present work presents the necessary extensions to the HMB2 CFD solver of Liverpool to allow modelling of Gurney flaps either fixed or actuated. Several methods of implementing Gurney flaps were investigated, and it was found that modelling the flap as a discontinuity in the mesh produced results close to what Gurney flaps of some thickness would give. This also allowed a simple implementation of actuated Gurneys and the method is demonstrated here for 2D sections, finite span wings, and rotors in hover and forward flight.

If a Gurney flap is to be added to a rotor blade, a passive device will lead to a fully deployed Gurney

through the whole azimuth as in the study of Min *et al.* [15], while an active Gurney could be deployed on demand. In that case, it could be fully deployed in hover flight to increase the lift capability of the rotor, while in forward flight it could be retracted at the advancing side and deployed actively at the retreating side of the rotor. Also, due to the practicalities of implementing Gurney flaps on rotors, several configurations are possible and the method presented can cope with these various flap designs. Two possible Gurney flap configurations are shown in Figure 1.

In the first configuration, the Gurney flap is allowed to move vertically above and below the aerofoil. One obvious drawback of this option, if the Gurney is not telescopic, is that to obtain even 2 to 3 %c Gurney flaps, these should be placed around the 90% chord of the aerofoil. This would reduce the overall effectiveness of a fixed sized Gurney as discussed in the study of Li *et al.* [17]. Configuration (b) is hinged at the trailing edge of the lower surface and the Gurney is closed by rotating clockwise towards the leading edge.

Table 1 presents the most recent numerical studies related to rotors with Gurney flaps. As can be seen those studies can be divided to three categories. Studies which derive conclusions regarding the helicopter rotors based on 2D aerodynamics can be compared against others which use full rotor geometries. Moreover, different turbulent models are used, while the last difference is observed on the way that the Gurney flap was modelled. Last row of Table 1 summarises some of the limitations and questions arisen on the previous studies using the variable boundary condition technique to model the Gurney flap, and that will be addressed in this paper.

To our knowledge, the proposed method is the only published technique that preserves the physics of the flow near the Gurney flap without having to use the exact geometry of the thick Gurney. To demonstrate and substantiate this claim we shown not only integrated loads (as common in the literature) but also detailed flow fields that are rarely shown in published works.

II.   Numerical Methods

A.   HMB2 flow solver

The HMB2 CFD solver [18–20] was employed for this work. HMB2 solves the Navier-Stokes equations in integral form using the arbitrary Lagrangian Eulerian formulation for time-dependent domains with moving boundaries:

$$\frac{\mathrm{d}}{\mathrm{d}t} \int_{V(t)} \vec{w} dV + \int_{\partial V(t)} (\vec{F_\mathrm{i}}(\vec{w}) - \vec{F_\mathrm{v}}(\vec{w})) \vec{n} dS = \vec{S}. \tag{1}$$

The above equations form a system of conservation laws for any time-dependent control volume $V(t)$ with boundary $\partial V(t)$ and outward unit normal $\vec{n}$. The vector of conserved variables is denoted by $\vec{w} = [\rho, \rho u, \rho v, \rho w, \rho E]^T$, where ρ is the density, u, v, w are the Cartesian velocity components and E is the total

internal energy per unit mass. $\vec{F}_\mathrm{i}$ and $\vec{F}_\mathrm{v}$ are the inviscid and viscous fluxes, respectively. For hovering rotors, the grid is fixed, and a source term, $\vec{S} = [0, -\rho\vec{\omega} \times \vec{u}_\mathrm{h}, 0]^T$, is added to compensate for the inertial effects of the rotation. $\vec{u}_\mathrm{h}$ is the local velocity field in the rotor-fixed frame of reference.

The non-inertial frame of reference used here has two benefits over a rotating frame of reference: firstly, the energy equation is unchanged by the rotation vector $\vec{\omega}$ and, secondly, a vanishing 'undisturbed' velocity field occurs in contrast to the position-dependent 'undisturbed' velocity field in the rotating frame of reference, which is given by $-\omega \times \vec{r}$.

Equations (1) are discretized using a cell-centred finite volume approach on structured multiblock grids. The spatial discretisation leads to a set of equations in time,

$$\frac{\partial}{\partial t}(\vec{w}_{\mathrm{i,j,k}} V_{\mathrm{i,j,k}}) = -\vec{R}_{\mathrm{i,j,k}}(\vec{w}_{\mathrm{i,j,k}}), \tag{2}$$

where $\vec{w}$ and $\vec{R}$ are the vectors of cell variables and residuals, respectively. Here, i,j,k are the cells indices in each of the grid blocks, and $V_{\mathrm{i,j,k}}$ is the cell volume. The convective terms are discretized using Osher's upwind scheme [21], MUSCL variable interpolation is used to provide high order accuracy and the Van Albada limiter [22] is employed to prevent spurious oscillations near steep gradients. Boundary conditions are set using ghost cells on the exterior of the computational domain. For viscous flow simulations, ghost values are extrapolated at solid boundaries ensuring that the velocity takes on the solid wall velocity. Implicit time integration is employed, and the resulting linear system of equations is solved using a pre-conditioned Generalised Conjugate Gradient method. For unsteady simulations, an implicit dual-time stepping method is used, based on the pseudo-time integration approach by Jameson [23]. The HMB2 method has been validated for a range of rotorcraft applications and has demonstrated good accuracy and efficiency for very demanding flows. Examples of work with HMB2 can be found in references [18], [19], [24]. Several rotor trimming methods are available in HMB2 along with a blade-actuation algorithm that allows for the near-blade grid quality to be maintained on deforming meshes [18].

The HMB2 solver has a library of turbulence closures including several one- and two- equation turbulence models and even non-Boussinesq versions of the $k - \omega$ model that is used for this work. Turbulence simulation is also possible using either the Large-Eddy or the Detached-Eddy approach. The solver was designed with parallel execution in mind and the MPI library along with a load-balancing algorithm are used to this end. For multi-block grid generation, the ICEM-CFD Hexa commercial meshing tool is used and CFD rotor grids with 10-30 million points and thousands of blocks are commonly used.

For forward flying rotors, the HMB2 solves the compressible-flow Reynolds-Averaged Navier-Stokes equations in an inertial frame of reference. The employed finite-volume discretisation accounts for moving and deforming meshes in time-accurate simulations. Consequently, a rotor in forward flight is modelled in a

'helicopter-fixed frame of reference', where the forward flight velocity is introduced through the definition of the 'free-stream' conditions. For isolated rotors, as well as, rotor/fuselage or rotor/wind-tunnel cases, the rotor and rotor blade motions are then accounted for using mesh velocities. For rotor/fuselage or rotor/wind-tunnel cases, the relative motion of the rotor and the fixed fuselage or tunnel is accounted for the sliding-plane approach [19].

B.   Proposed methods for Gurney flap modelling

The proposed methods for dealing with the Gurney flaps of Figure 1 and 2 are outlined below. It should be noted that the first two methods can be implemented using part of the functionality required in overset grid methods, namely the ability to apply wall boundary conditions to any cell face when the overset grids intersect each other, and the ability to cut a hole into a grid where there is an intersection with a solid. This is shown in the second method in Figure 2b.

The first method (Figure 2a) uses the *current grid lines* within the block. In the past, when using HMB2, fixed Gurneys have been approximated by setting a solid wall boundary flag between blocks, giving the effect of a very thin flap. The code had to be extended for the active Gurney case. As an example, consider configuration shown in Figure 1a for a case where a Gurney is aligned with a block boundary. As the Gurney moves, it will violate the requirement of HMB2 CFD solver to have a single boundary condition on each block face. In Figure 2a as the Gurney rotates it will need to swap over from one grid line to the next. The configurations of Figure 1 would be possible if the CFD method allows any face within a block to be flagged as a solid wall.

The second method (Figure 2b) is one step closer to the overset grid method. Here *cells are flagged as solid* if they contain part of the flap. In addition to the functionality of the first method (the ability to flag any cell face as a solid wall) the second method also requires a way of flagging cells, in this case shown in shade (Figure 2b), as non computational cells or holes. After these holes have been flagged it is a matter of finding any face that is connected to both a computational cell and a hole, and flag that as a solid wall.

The final method (Figure 2c) is to use *two overset grids*. One associated with the aerofoil and the second associated with the active Gurney. This requires all the functionality of the first two methods with additional information needed within HMB2. Firstly, it is necessary to know which cells in each grid are going to be used for computing the solution. For example, if the choice is the background grid with the minimum number of holes, one needs to know how far does the under resolved flow next to the Gurney affect the rest of the background solution. HMB2 then requires two extra pieces of information, firstly which cells are used in the computational domain, and secondly how is information exchanged between grids.

The problem with moving Gurney flaps is that the solid surface of the Gurney which is surrounded by

a fine CFD mesh to resolve the flow, will have to come very close to the mesh around the aerofoil. The high aspect ratio and very fine grids required to resolve boundary layer flows made the use of some of the proposed methods difficult.

III.   Implementation of the Gurney flaps

This section discusses the different methods of modelling a Gurney flap, each with its own advantages and disadvantages.

A.   Gurney flap modelled within the multi-block mesh

The most natural way to solve a fixed steady state Gurney flap is to include the Gurney within the multiblock grid as shown in Figure 3. In this case, the Gurney flap has a well resolved wall spacing on all sides and hence will be a benchmark solution for comparing it with solutions where the Gurney flap is approximated.

To obtain the loads on the Gurney flap alone and to be able to find its moment about a different point - for example the Gurney hinge two additional pieces of information are required. Firstly, a special boundary condition tag is used so the Gurney flap is identified. Secondly, additional Gurney-specific input is necessary to inform the CFD solver that computations are to be performed with a Gurney flap of a specific actuation. Figure 3b shows the two boundaries that need to be integrated separately for the calculation of the loads. The boundary for the aerofoil is highlighted with the solid line with the black dots, while the Gurney flap boundary is shown as the solid line with the white gradient symbol.

B.   Gurney flap modelled using viscous wall boundary condition across a block face

In this case the Gurney is assumed to be thin, and is modelled along a block boundary. Since it is a restriction within HMB2 that each block face can only have one type of condition applied to it, the whole face must be part of the Gurney flap. The case, however, is computed in exactly the same way as if the Gurney had some thickness as explained in section A. The advantage of this method is that no additional effort is needed in terms of mesh generation. On the other hand, the Gurney is assumed to have no thickness and its size must coincide with the size of a block face. Figures 4 and 5 present the concept along with its extension to several cases discussed below.

C.   Gurney flap modelled using blocked cells next to a block face

To overcome the restrictions of the previous method regarding the size of the Gurney flap, a new way of modelling thin Gurneys has been added to HMB2. This allows for any number of cells on a block face to be flagged as blocked. This means that the same grid can be used for different size flaps as well as

allowing unsteady deployment of Gurney flaps along block interfaces. Figures 4 and 5 present the idea using schematics of cells and block interfaces.

For an actuated Gurney it is important to have a robust method for blocking the correct cells. This process can be framed as a collection of computational geometry problems which have to work robustly in the very thin, high aspect ratio, cells that make up the first part of any boundary layer mesh. The algorithm is a four stage process.

Part one is to define a planar Gurney with three points, the remaining stages are then computational geometry problems which eliminate cells until just those representing the Gurney remain. Figure 4 explains how the cell faces are finally flagged as a Gurney flap. First, the block boundaries 3 and 4 are excluded as they do not meet the distance requirements between the centroid of each cell face and the planar Gurney, set by the user. Then, parts of the boundaries 1 and 2 which are inside a circle are also excluded as the angle between the normal to the face and the normal to the Gurney does not meet another user specified tolerance. Finally, the remaining cell centres of the faces are projected onto the Gurney plane and if they are inside the polygon formed by the Gurney they are flagged as blocked. These cells are surrounded by the dashed line at the trailing edge of the aerofoil shown in Figure 4b. This algorithm can be seen below in the flow chart of Algorithm 1.

Data: Define the Gurney as a set of points.
forall the *blocks in the mesh* **do**
    forall the *internal boundaries of each block* **do**
        forall the *faces on each internal boundaries* **do**
            if *the centroid of the face is close to the Gurney* **then**
                if *the normal to the Gurney nearly parallel to the normal of the face* **then**
                    if *the centroid of the face inside the polygon of the Gurney* **then**
                        Flag this face as in the Gurney flap
                    end
                end
            end
        end
    end
end

Algorithm 1: Flow chart for Gurney flap definition.

1. Resolution of the length of the Gurney

For a Gurney flap of fixed height it is always possible to place a grid point at the end of the Gurney and hence no approximation is made if the method of blocked cell faces is used. However, if the Gurney does not end at a grid point the semi-blocked cells must be treated in a special way. The first method is as follows: if the projection of the centre of a cell faces onto the plane described by the Gurney flap is within the Gurney,

then it is flagged as blocked else it is flagged as open. Examples of this method were shown in Figures 5a -
5f. The Gurney, shown in bold solid line, is assumed to be infinity thin and close to a block boundary the
shaded cells are flagged and a viscous wall boundary condition is applied to the face that coincides with the
Gurney. Figures 5a - 5f show that as the Gurney extends in length, more of the cells are flagged as blocked.
The length of the Gurney can only be resolved to the size of the mesh cell at its end.

To demonstrate this behaviour, three cases were computed using a Gurney at the trailing edge of a
NACA0012 aerofoil of a length approximately 1% of the aerofoil chord. Figures 5g, 5h, and 5i show the grid
and the region around the end of the Gurney and the results are presented in Table 2. It can be seen that
this grid has a large number of points normal to the Gurney surface to help resolve the flow.

The discretisation effect of an actuated Gurney flap was addressed with a technique that allows the flux
between cells to be split according to the area of a cell exposed to the flow. The idea is to compute first the
fraction of the area covered by the Gurney flap over the area of the cell face. The flux f_1 is computed on
the interface between the two cells assuming no wall, and then, the flux f_2 is computed as if there is a wall
boundary at the face of the cell. Finally, these fluxes are weighted by the fraction of the areas as described
in the following equation:

$$f = f_1 \cdot (1 - \Delta A) + f_2 \cdot \Delta A \tag{3}$$

An example of the part-flux method is shown in Figure 6. In Figure 6a a simple schematic of two cells
is presented where a Gurney flap covers the shaded area. Figure 6b presents how these cells are treated in
the code during the two different calculations of the fluxes before weighting them.

Figures 7, 8 present the comparison of the results obtained for a NACA0012 with a 2% chord actuated
Gurney flap between the full-flux and the part-flux method. Judging from Figure 7 the variation of the
change of the lift coefficient of the aerofoil is smoother when it is computed with the part-flux method (solid
line), while with the full-flux method rapid changes of the lift are observed while changing the size of the
Gurney flap (dotted line). In Figures 8a, b the U and V components of the velocity are presented near the
Gurney flap with contours for the full-flux method and lines for the part-flux method.

D.   Swinging Gurney

For such a case a blocking topology is seen in Figure 9. The Figure shows the mesh around a NACA0012
aerofoil with a swinging Gurney located at 95% of the chord and the modification of the blocks near the
trailing edge of the aerofoil.

The method used to flag cell faces as blocked for a swinging Gurney is described in Algorithm 2 and
is presented in Figures 9 and 10. First, the code calculates the radius of the Gurney in the same way it

Find the radius of the Gurney
Find the angle of the Gurney
forall the *swinging Gurney blocks in the mesh* **do**
    if *the point is inside the radius* **then**
        Flag the cells behind and in front of the Gurney with -1 and 1
    else
        Flag the cells behind and in front of the Gurney with -2 and 2
    end
end
Sweep along the lines
if *the sign changes between two cells* **then**
    if *the sum of the four neighbour cells of a node is 6* **then**
        This node is the end of the Gurney flap
    end
end
All the cell faces up to that node will be flagged as blocked

Algorithm 2: Flow chart for swinging Gurney flap definition.

calculated the height of the Gurney during the linear actuation. At every time step, it then computes the

angle of the Gurney and it defines the new Gurney plane as shown in Figure 10a. The block topology for a

swinging Gurney case is presented in Figure 9. Then for the blocks $1 - 4$ in the near view of Figure 9 the

code flags the cells behind and in front of the Gurney with -1 and 1 respectively if they are inside the radius

of the Gurney or with -2 and 2 if they are outside as presented in Figure 10b. Next, the code sweeps along

the grid lines and averages the flags on the nodes. The nodes with zero value will form the Gurney flap, and

if the sum of the absolute values of the four neighbour cells of a node is 6 then this node is the end of the

Gurney flap as presented in Figures 9c, d. Then all the cell faces up to the end point are flagged as blocked.

IV.   Results for Gurney flaps in two dimensions

The following section demonstrates the different methods for modelling Gurney flaps that were outlined

in section III.

A.   Fixed Gurney flap

The grid used for these calculations can be seen in Figure 11. The aerofoil used is a NACA0012 at $\alpha = 0^o$,

$M = 0.2$, and $Re = 2.1 \cdot 10^6$. Different Gurney sizes were used from 0.5%c up to 2%c, and the span of the

Gurney was 1 chord. The aerofoil trailing edge was refined more than the normal to resolve the boundary

layer of the Gurney and the vortical flow structures downstream. The normal spacing to the surface of the

aerofoil is $5.0 \times 10^{-6}c$ which is about an order of magnitude less than that the normal spacing to the Gurney

flap. As can be seen in Figure 11(c) the block near the trailing edges extends in the normal direction by 2%

of the chord and has been expanded in such a way so that the cells are nearly equally spaced. This is unlike

a normal aerofoil grid where the cells would keep expanding, consequently these blocks have a large number of cells. This will give a good approximation of any Gurney flap up to a height of 2% c. The block after the trailing edge between $x/c = (1.01, 1.07)$ has a constant spacing in the x-direction again to help capture the vortical flow in the wake. The same grid was used for all calculations and the flow cases were run as discussed in section III-C.

Figure 12 shows the pressure and streamlines for four different Gurney flap sizes at conditions $M = 0.2$, $\alpha = 0^o$, and $Re = 2.1\text{x}10^6$. As the Gurney increases in size, the pressure difference between the two sides of the Gurney also increases and the flow acceleration near the trailing edge increases reducing the pressure behind the Gurney. The pressure in front of the Gurney increases due to the larger pocket of stagnant flow.

B. Resolving flow details near the Gurney flap

Several of the works published in the literature tend to model Gurney flaps using simple flow blockage that did not result in fully resolved flows. In this section, the results obtained with HMB2 for an aerofoil section near a fixed Gurney are put forward as an example of the resolution that should be sought for the Gurney flap computations. This requires fine grids but shows clearly the capability of HMB2 in resolving the details of the flow and the results presented here should be considered as a benchmark to gauge the correct mesh resolution. In the present study a C-type mesh of $195,000$ nodes is used, 221 nodes were used in the normal direction to the surface with the spacing close to the wall being $1.0 \times 10^{-5}c$, and 189 in the wake with 80% of them used up to 50%c distance from the trailing edge. This was necessary to capture the vortices created behind the Gurney flap. Figure 13 shows several views of the flow near the corner of the Gurney flap. Pressure contours and streamlines are combined to show the successive resolution of the corner vortices expected in the aerofoil Gurney junction.

The mesh resolution is equally important behind the Gurney flap and near the trailing edge of the section especially since a blunt trailing edge is modelled. This can be seen in Figure 14 where both pressure and turbulent Reynolds number fields are shown again for an NACA0012 aerofoil with a 2%c flap near the trailing edge. A further comparison is shown in Figure 15 where results from computations for an infinitely thin Gurney are compared against results at the same conditions but for a Gurney with finite thickness. Such comparisons suggest that for most cases the infinitely thin Gurney gives a well-resolved representation of the flow and allows easier implementation in HMB2.

Results are obtained for 2% c Gurney flap located at 95%c of a NACA0012 aerofoil. For this case, some experimental data are available [1,17] and the comparisons are presented in Figure 16. For the clean aerofoil the CFD results agree well with the experiments. As the size of the Gurney flap increases there is a small overestimation of the lift and underestimation of the moment, while this difference grows as the aerofoil

pitches up. In Figure 17 the results for Gurney size 2%c show that the pressure distribution at the suction side of the aerofoil at zero degrees of incidence is under-predicted, which leads to discrepancies in the lift coefficient.

C.   Comparison against thick Gurney flap

Next, a NACA23012M aerofoil with a cavity at the trailing edge was tested actuating a virtual Gurney flap linearly. The reduced frequency selected for the oscillation of the flap was $k = 0.1$ and the period of the oscillation was 10π travel times. A non dimensional timestep of 0.001 was used. Figure 18 presents the way the Gurney is flagged and actuated. In Figure 18a the Gurney is fully retracted inside the cavity, while in Figure 18b it is fully deployed and it is extended by 1.5%c outside the cavity. However, the Gurney still exists inside the cavity as the hinge is always attached to the upper wall of the cavity. When the Gurney is retracted its actual size is 53.9% of the fully deployed Gurney.

Next, the unsteady computation of an actuated Gurney of 1.5%c at 0.935c of a NACA23012M aerofoil with a cavity was compared against the same case with a thick Gurney using the Chimera technique. Figure 19 presents the unsteady loads for these two cases, while in Figures 20, 21, 22 vorticity contours are presented for three different time steps. As can be seen behind the Gurney flap the vorticity magnitude shows no difference. The only difference is observed inside the cavity where it is assumed to be split into two cavities when the virtual Gurney is used. When the thick Gurney is implemented with the Chimera technique the flow is allowed to circulated around the gunrey inside the cavity too.

V.   Results for Gurney flaps on wings in three dimensions

Since the two dimensional NACA0012 results over-predicted the lift generated via the Gurney flap the case has been extended to an infinite rectangular wing, via symmetry boundary conditions, with a finite span Gurney. As can be seen from the surface mesh in Figure 23 the wing has a span of 1.6 chords with the Gurney starting at 0.24 z/c and finishing at 1.36 z/c. This makes the Gurney cover 70% of the span of the wing with 15% gap before the symmetry boundary conditions are applied. The edges of the Gurney have only slightly be refined with a spacing of $1.0 \times 10^{-3}c$ which is approximately 1/20 of the height of the Gurney flap. This means that the flow will not be close to being resolved in this region but the confinement of the two dimensional flow will be removed. The test case was a NACA0012 at zero angle of attack with a Reynolds number of 2.1 million and a Mach number of 0.2 to approximate the low speed flow used in the experiment. Figure 17 shows the differences in pressure when comparing with the two dimensional results as well as the experimental data [1, 17]. The pressure distribution on the NACA0012 at zero pitch is well known and it does not agree with the experiments, which overpredict the pressure compared to Ladson's et

al. study [25]. It seems that there are strong wind tunnel effects which resulted in the discrepancies between the experiment and the CFD results. The use of a three dimensional calculation has reduced the difference between upper and lower surface pressure so that now CFD is much closer to the experimental data. The offset between CFD and experiments now is also close to the offset seen between the case where no Gurney was used. The stagnation pressure in front of the Gurney is the same for both the two and three dimensional cases but the upper surface is flatter for 3D more in line with the experiment.

Indicative results for the wing case with a fixed Gurney flap can be seen in Figures 24 a, c, e. The Oscillating the Gurney added another slow varying change in the integrated loads. These results are presented Figures 24 b, d, f. The lift coefficient corresponds to the total lift of the wing, while the drag coefficient corresponds to the pressure and viscous drag on the Gurney flap.

For the same case of the NACA0012 wing at zero angle of attack with a Reynolds number of 2.1 million and a Mach number of 0.2 a swinging Gurney was actuated between 45° and 135°, and the results obtained are presented in Figure 25. It is mentioned that when the Gurney is located at 90° it is normal to the mean chord line. Both the mean lift and drag coefficients were decreased for the case of the swinging Gurney, but it proved to introduce high frequency changes to the pressure at the suction side of the wing towards the leading edge.

VI.   Results for Gurney flaps on Rotors

Although, this is not a study on the effect of Gurney flaps on rotor performance, the UH-60A rotor was tested in hover and forward flight in order to prove the effect and the robustness of the proposed method at different flight conditions.

A.   Mesh and implementation

For all rotor cases shown, the grid has not been developed with running with a Gurney flap in mind. This means that the Gurneys will not be well-approximated by the block interface. The span-wise resolution will be poor with most cases only a handful of cells being used in the span-wise direction. The active Gurneys will not have well approximated lengths since the last couple of cells in the boundary layer mesh will make up nearly 50% of the total Gurney length. However, these are very good grids to test the robustness of the flagging algorithm since all these problems makes marking which faces are to be included in the Gurney more difficult.

If the steady state formulation of the hover method is used within HMB2, it is not possible to actuate the Gurney flap. In hover, the Gurney flap must be specified using the global coordinates of the blade just as in the 2D and 3D wing cases and a fixed deployment should be assigned to it. Figure 26 shows two Gurneys

on the back of a UH60A rotor. As can be seen from figure 26a It is possible for a Gurney to span more than one block faces, as well as, to have multiple Gurneys within a single block. However, it is not possible to have multiple Gurneys within a single cell face since this case this face would be double accounted for once for each Gurney. It can be seen in figure 26b that the mesh was not designed with a Gurney in mind for example the lack of orthogonality to the rotor surface at the most outboard cell faces.

Defining the Gurney in a forward flight case mirrors the way this is done for the active flaps with HMB2 [26]. For example, the hinge line of the Gurney must go through a complete revolution with the flap, lag and pitch harmonics included in the articulation. To remove this problem from HMB2 a "reference" frame is used. This reference frame has the build in coning collective and linear twist removed. The difference between the two systems can be seen in Figures 27a, 27b. The other obvious change is that now all 4 blades lie on top of each other. This means that for a forward flight, if there is a single Gurney per blade only one has to be defined in the reference frame. Figures 27c, 27d show more clearly the differences between the blade at azimuth zero in the global and reference frames. It is not possible to apply a Gurney flap that does not have at least one face on the rigid hull. So for the case of rotor blades modelled as having sharp trailing edges it is not possible to apply a Gurney extending horizontally unless the blocks behind the trailing edge are included in the rigid hull. This limitation does not apply to rotor blades with blunt trailing edge.

Since the flagging of the Gurney is purely a geometric problem the cells next to the blade need careful consideration. A Gurney flap of large span just defined at the two edge points. If, however, there is a very slight curve in the trailing edge of the rotor cells can be missed in the Gurney or spurious cells can be flagged on the wrong surface. An example of this is shown in Figure 28. A close view of the outboard Gurney shows cells next to the blade that failed to be flagged. This problem can be removed in a couple of ways. Firstly, the Gurney can be split into two so the straight line segments of the Gurney better approximate the trailing edge. The second method is to add extra points along the trailing edge in order to change the representation of the Gurney from a quadrilateral to an n-sided polygon as it is shown in Figure 29.

In this case one extra point was added in the middle of the Gurney and Figure 30(a) shows that the hole is removed. Figure 30b shows the z component of the velocity on the blade and the Gurney flap. As can be seen the wall-Face boundaries clearly pick up the correct velocity, however, it should be noted the velocity due to the motion of the Gurney itself is currently not applied in any configuration. This effect is expected to be small for a linear actuation mode.

B.   UH60A rotor in hover and forward flight with two Gurney flaps

To demonstrate the capability of modelling Gurney flaps in HMB2, the UH60A rotor was analysed in hover, with and without Gurney flaps. The flaps were placed at the position shown in Figure 30. The locations

of the flaps were specified in the HMB2 input files and the computation was run for at least 20,000 steps. The surface pressure coefficient on the clean and flapped blades is shown in Figure 31 and as can be seen the influence of the flap is extended on the upper and lower surfaces as expected. The effect of the flap is localised and it seems to decay rapidly away from the tips. The Gurney enhanced the lifting of the blade but at the same time, it increased torque and pitching moments. This result was expected since Gurneys are known to have poor moments and when compared to trailing edge flaps they suffer from higher drag penalty for the same effect on the lift. On the other hand, the size, place and extension of the Gurney were not optimised. The effect of the Gurney on the surface pressure coefficient of blade is shown in Figure 32. The additional vortices due to the Gurney flaps are also visualised using the Q-criterion.

The UH60A rotor analysed by Steijl and Barakos [19] was also used with an active Gurney in forward flight. The CFD was initially relatively coarse as it was used to demonstrate the method of implementing Gurney flaps within HMB solver. The size of the Gurney used was $2.2\%c$ and the span of the Gurney was $0.465c$. $M_\infty = 0.2363$, $Re = 5\mathrm{x}10^6$, and advance ratio $\mu = 0.368$ were used for the calculations. A 1/Rev actuation schedule was used, which is presented in Figure 33. Here, the Gurney flap is retracted at $\Psi = 90^o$, while it is 50% deployed at $\Psi = 0^o$ and $\Psi = 180^o$, and reaches full deployment at $\Psi = 270^o$. Figure 35 presents the surface pressure coefficient on the clean and flapped blades. The effect of the Gurney is visible at 0, 180 and 270 degrees of azimuth as expected by the employed actuation schedule. As was the case for the hovering rotor, the span-wise effect of the flap appears to decay rapidly. The strongest effect in terms of normal force is captured at the front and the back of the disk, while negative moments are introduced around the whole azimuth, apart from the area close to $\Psi = 90^o$. As far as the torque is concerned, it increases significantly in the last quarter of the azimuth and always close to the location where the Gurney is deployed. For these calculations an elastic blade was considered and the results were compared against experimental data obtained from Coleman and Bousman [27] and for the clean rotor case they show fair agreement. Figure 34 presents the lift and moment distribution at $0.675R$ and $0.865R$ sections around the azimuth for the clean rotor and the rotor with Gurney after having subtracted the mean values. Although the size of the Gurney flaps is not big enough to change dramatically the normal force distribution of the section it seems that it affects the pitching moment at $0.865R$ section. The integrated loads of the disk for the elastic rotor can be seen in Figure 36. For the case of the deployment of the Gurney at the suction side of the blade (Figure 37) the lift of the clean rotor is decreased but there is a benefit on the moments as most of the previous nose-down pitching moments disappeared. Tables 3, 4 present the effect of the Gurney flap on the mean and peak-to-peak values of the integrated loads. In general, for any rotor high average thrust values are expected in terms of the integrated normal force loads, while the blade pitching moments and the torque should remain low. As far as the peak to peak values goes, all of them should remain low and

especially the torque, as the requirements for the engine are not expected to face big changes around the azimuth. For the UH-60A rotor case the Gurney flap increases the thrust capability of the rotor by 7.4% but the average nose down pitching moment of the blade around the azimuth is increased by 20%. At the same time the torque is increased by 4%.

VII. Conclusions and the Future Work

This work discussed the functionality added to HMB2 for modelling Gurney flaps. Out of the approaches outlined at the beginning of the paper, none delivered completely the ability to model any Gurney flap at any configuration and actuation profile. However, the final method allows to linear and swinging Gurney flaps to be analysed.

For 2D cases the differences between Gurney flaps with finite thickness and infinitely thin Gurneys were highlighted. It was found that the loads and the flow physics near the Gurney are well captured by the infinitely thin Gurneys and this encouraged the development of a method where the Gurney is placed on a block boundary and is sliding in and out of the surface. A separate investigation was conducted to quantify the effect of having Gurney flaps covering parts of CFD cells. Modelling part-cell fluxes in HMB2 was difficult but the results showed better predictions for the loads with smoother variations as the Gurney did not have to "jump" between cells. The method allows to re-cycle grids with minimal modifications and captures the flow physics of the Gurney. The method was also tested for 3D cases including rotors in hover and forward flight. For the forward flight case actuated Gurneys were used. The validation of the methods was limited since the code provided efficient solutions that were not compared against any test data, however, the overall flow features seemed reasonable and agreed with the broad understanding of the rotors for the effect of Gurneys on aerofoil aerodynamics. For wing cases, part-span Gurneys were inserted in a low aspect ratio wing based on the NACA0012 section and the results showed the formation of tip vortices at the ends of the Gurney flap. The Gurney had a significant effect on the aerodynamics of both pressure and suction sides. Unfortunately, no data were available to validate the predictions. Finally, the method was used for forward flight and hovering rotors using the UH60A blade as the starting point. Two Gurneys were added to the blade and results were obtained with and without the active Gurneys. The results suggested that the convergence of HMB2 was not significantly affected by the Gurneys and regardless of the small size of the flaps, some effect on the loads and flow was noticed. To validate the results, experiments in the open literature were sought for the purposes of this project. Very few sets were found mainly related to flaps that were fixed. For active flaps there was only one source of data identified for a wing in tunnel case. The results obtained with HMB2 were in fair agreement with the experiments showing some limitations of the tunnel test.

Further enhancements of the capability of HMB2 to model lifting surfaces with active Gurney flaps are planned. At first, more effort is being directed towards the HMB2 chimera implementation for Gurney flaps. The need for validation data is obvious based on the progress made with the CFD simulations. What is necessary is a small targeted experiment that will provide active Gurney results for a full-span flap on a wing as well as some data for a part-span Gurney. The results could be for a linearly actuated or for a pivoted Gurney. It is much harder to obtain good data for rotors but this should be attempted at least for a simple rotor case. Given the lack of any data in the literature, an experiment that provided even integrated loads for a rotor equipped with a Gurney would be very useful for the validation of HMB2 and other CFD methods.

References

[1]Wang, J. J., Li, Y. C., and Choi, K. S., "Gurney flap - Lift enhancement, mechanisms and applications," *Progress in Aerospace Sciences*, Vol. 44, 2008, pp. 22–47.

[2]Liebeck, R. H., "Design of Subsonic Airfoils for High Lift," *Journal of Aircraft*, Vol. 15, No. 9, Sept 1978, pp. 547–561.

[3]Jeffrey, D. and Zghang, X., "Aerodynamics of Gurney Flaps on a Single-Element High-Lift Wing," *Journal of Aircraft*, Vol. 37, No. 2, March-April 2000, pp. 295–301.

[4]Troolin, D., Longmire, E., and Lai, W., "Time Resolved PIV Analysis of Flow over a NACA 0015 Airfoil with Gurney Flap," *Experiments in Fluids*, Vol. 41, 2006, pp. 241–254.

[5]Lee, T. and Su, Y., "Lift Enhancement and Flow Structure of Airfoil with Joint Trailing-Edge Flap and Gurney Flap," *Experiments in Fluids*, Vol. 50, 2011, pp. 1671–1684.

[6]Tang, D. and Dowell, E., "Aerodynamic Loading for an Airfoil with an Oscillating Gurney Flap," *Journal of Aircraft*, Vol. 44, No. 4, July-August 2007, pp. 1245–1257.

[7]Chow, R. and van Dam, C. P., "Unsteady Computational Investigations of Deploying Load COntrol Microtabs," *Journal of Aircraft*, Vol. 43, No. 5, Sept–Oct 2006, pp. 1458–1469.

[8]Baker, J. P., Standish, K. J., and van Dam, C. P., "Two-Dimensional Wind Tunnel and Computational Investigation of a Microtab Modified Airfoil," *Journal of Aircraft*, Vol. 44, No. 2, March–April 2007, pp. 563–572.

[9]Kinzel, M. P., Maughmer, M. D., and Duque, E. P. N., "Numerical Investigation on the Aerodynamics of Oscillating Airfoils with Deployable Gurney Flaps," *AIAA Journal*, Vol. 48, No. 7, July 2010, pp. 14571469.

[10]Camocardi, M. E., Di Leo, J. M., Delnero, J. S., and Colman Lerner, J. L., "Experimental Study of A Naca 4412 Airfoil With Movable Gurney Flaps," *49th Aerospace Sciences Meeting including the New Horizons Forum and Aerospace Exposition*, 2011, AIAA-2011-1309.

[11]Lee, T., "PIV study of near-field tip vortex behind perforated Gurney flaps," *Experiments in Fluids*, Vol. 50, No. 2, 2011, pp. 351–361.

[12]Cole, J. A., Vieira, B. A. O., Coder, J. G., Premi, A., and Maughmer, M. D., "Experimental investigation into the effect of gurney flaps on various airfoils," *Journal of Aircraft*, Vol. 50, No. 4, 2013, pp. 1287–1294.

[13]Yee, K., Joo, W., and Lee, D. H., "Aerodynamic Performance Analysis of a Gurney Flap for Rotorcraft Applications," *Journal of Aircraft*, Vol. 44, No. 3, May–June 2007, pp. 1003–1014.

[14]Liu, L., Padthe, A. K., and Friedmann, P. P., "Computational Study of Microflaps with Application to Vibration Reduction in Helicopter Rotors," *AIAA Journal*, Vol. 49, No. 7, July 2011, pp. 14501465.

[15]Min, B., Sankar, L. N., Rajmohan, N., and Prasad, J. V. R., "Computational investigation of Gurney flap effects on rotors in forward flight," *Journal of Aircraft*, Vol. 46, No. 6, 2009, pp. 1957–1964.

[16]Palacios, J., Kinzel, M., Overmeyer, A., and Szefi, J., "Active Gurney Flaps: Their application in a Rotor Blade Centrifugal Field," *Journal of Aircraft*, Vol. 51, No. 2, March–April 2014.

[17]Li, Y., Wang, J., and Zhang, P., "Effects of Gurney Flaps on a NACA0012 Airfoil," *Flow, Turbulence and Combustion*, Vol. 68, 2002, pp. 27–39.

[18]R. Steijl, G. Barakos and K. Badcock, "A framework for CFD analysis of helicopter rotors in hover and forward flight," *International Journal for Numerical Methods in Fluids*, Vol. 51, No. 8, 2006, pp. 819–847.

[19]Steijl, R. and Barakos, G., "Sliding Mesh Algorithm for CFD Analysis of Helicopter Rotor-Fuselage Aerodynamics," *Int. J. Numer. Meth. Fluids*, Vol. 58, 2008, pp. 527–549.

[20]Barakos, G., Steijl, R., Badcock, K., and Brocklehurst, A., "Development of CFD Capability for Full Helicopter Engineering Analysis." 31st European Rotorcraft Forum, 13-15 September 2005, Florence, Italy, 2005.

[21]Osher, S. and Chakravarthy, S., "Upwind schemes and boundary conditions with applications to Euler equationsin general geometries," *Journal of Computational Physics*, , No. 50, 1983, pp. pp. 447–481.

[22]Albada, G. D. V., Leer, B. V., and Roberts, W., "A comparative study of computational methods in cosmic gas dynamics," *Astronomy and Astrophysics*, Vol. 108, 1982, pp. pp. 76.

[23]Jameson, A., "Time Dependent Calculations Using Multigrid, with Applications to Unsteady Flows Past Airfoils and Wings," 1991, AIAA-91-1596.

[24]Steijl, R. and Barakos, G., "A Computational Study of the Advancing Side Lift Phase Problem," *Journal of Aircraft*, Vol. 45, No. 1, 2008, pp. 246–257.

[25]Ladson, C. L., Hill, A. S., and Johnson, W. G. J., "Pressure Distributions from High Reynolds Number Transonic Tests of an NACA 0012 Airfoil in the Langley 0.3-Meter Transonic Cryogenic Tunnel," *NASA TM 100526*, December 1986.

[26]Steijl, R., Woodgate, M., and Barakos, G., "CFD method for efficient analysis of flapped rotors," 2010, pp. 505–517.

[27]Coleman, C. and Bousman, W., "Aerodynamic limitations of the UH-60A Rotor," *NASA Technical Memorandum NASA TM-110396*, 1996.

[28]Min, B. Y., Sankar, L., and Bauchau, O. A., "A CSD-CFD Coupled Analysis of Hart-II Rotor Vibration Reduction using Gurney Flaps," *American Helicopter Society 66th Annual Forum, Phoenix, AZ, May 11–13*, 2010.

[29]Matalanis, C. G., Wake, B. E., Opoku, D., Min, B. Y., Yeshala, N., and Sankar, L., "Aerodynamic Evaluation of Miniature Trailing-Edge Effectors for Active Rotor Control," *Journal of Aircraft*, Vol. 48, No. 3, May–June 2011.

[30]Bae, E. S. and Gandhi, F., "Upstream Active Gurney Flap for Rotorcraft Vibration Reduction," *American Helicopter Society 68th Annual Forum, Fort Worth, TX, May 1–3*, 2012.

[31]Pastrikakis, V. P., Steijl, R., and Barakos, G. N., "Computational Aeroelastic Analysis of a Hovering W3 Sokol Blade with Gurney Flap," *Journal of Fluids and Structures*, , No. 1763, 2014.

[32]Menter, F. R., "Two-equation eddy-viscosity turbulence models for engineering applications," *AIAA Journal*, Vol. 32, No. 8, 1994, pp. 1598–1605.

Title	Year/Authors	Model	Notes
"Computational Investigation of Gurney Flap Effects on Rotors in Forward Flight [15]"	2009/Byung-Young Min et al.	BO-105 blade	Spalart-Allmaras Detached Eddy Simulation k-ω turbulence model.
"Numerical Investigation on the Aerodynamics of Oscillating Airfoils with Deployable Gurney flaps [9]"	2010/Kinzel et al.	S903 aerofoil	Spalart-Allmaras turbulence model - Overset grids.
"A CSD-CFD Coupled Analysis of Hart-II Rotor Vibration Reduction using Gurney Flaps [28]"	2010/Byung-Young Min et al.	NACA0015, Hart-II blade	Spalart-Allmaras turbulence model - Variable boundary condition technique to model Gurney flap.
"Aerodynamic Evaluation of Miniature Trailing-Edge Effectors for Active Rotor Control [29]"	2011/Matalanis et al.	S903 aerofoil, UH-60A blade	Spalart-Allmaras turbulence model - Variable boundary condition technique to model Gurney flap.
"Computational Study of Microflaps with Application to Vibration Reduction in Helicopter Rotors [14]"	2011/Liu et al.	NACA0012 aerofoil	k-ω turbulence model - Overset grids.
"Upstream Active Gurney Flap for Rotorcraft Vibration Reduction [30]"	2012/Bae and Gandhi	SC-1095, SC-1094R8 aerofoils	The effect of active Gurney flaps on UH-60A rotor was examined using 2D aerodynamics.
"Computational Aeroelastic Analysis of a Hovering W3 Sokol Blade with Gurney Flap [31]"	2014/Pastrikakis et al.	NACA23012M aerofoil, W3-Sokol blade	k-ω SST turbulence model - Variable boundary condition technique to model Gurney flap.
"Active Gurney Flaps: Their application in a Rotor Blade Centrifugal Field [16]"	2014/Palacios et al.	S903 aerofoil, K-max blade	Spalart-Allmaras turbulence model - Overset grids.
Current study	2014/Woodgate et al.	NACA0012, NACA23012M aerofoils, NACA0012 wing, UH-60A blade	k-ω SST turbulence model - Variable boundary condition technique to model Gurney flap.
Limitations of previous using the variable boundary condition technique to model a Gurney flap	There is no detailed description of the algorithm used to model the Gurney flap. All studies accounted only for linearly actuated Gurney flaps. No clear evidence for capturing the vortex shedding behind the Gurney was provided. It is not clear how the grid quality is affected near the Gurney during the actuation of the flap. No comparison with a thick gurney in unsteady computations was performed. Low-amplitude high-frequency oscillations limitations were observed.		

Table 1. Numerical studies related to rotors with Gurney flaps.

Blocked Cells	Gurney Length % chord	Aerofoil Lift coefficient	Aerofoil Pressure Drag coefficient	Aerofoil Moment coefficient	Gurney Lift coefficient	Gurney Pressure Drag coefficient	Gurney Moment coefficient
58	1.0192-1.0292	0.2524	0.003762	-0.12026	0.0	0.004385	-2.101e-5
59	1.0292-1.0392	0.2611	0.003895	-0.12437	0.0	0.004699	-2.361e-5
60	1.0392-1.0492	0.2697	0.004031	-0.12843	0.0	0.005022	-2.641e-5

Table 2. Variation in the loads as the number of blocked cells increases using the baseline method.

Case	M^2Cn	M^2Cm	M^2Cq
Rigid Coarse Clean	0.07603	-0.00579	0.01328
Rigid Coarse Gurney	0.07941	-0.00682	0.01368
Elastic Coarse Clean	0.07041	-0.00540	0.01398
Elastic Coarse Gurney	0.07563	-0.00648	0.01455

Table 3. Pressure-based mean values of integrated loads for UH60-A rotor in forward flight.

Case	M^2Cn	M^2Cm	M^2Cq
Rigid Coarse Clean	0.27856	0.05091	0.038269
Rigid Coarse Gurney	0.31113	0.05143	0.038282
Elastic Coarse Clean	0.38765	0.05317	0.045850
Elastic Coarse Gurney	0.42630	0.05785	0.046060

Table 4. Pressure-based peak to peak values of integrated loads for UH60-A rotor in forward flight.

Configuration (a)
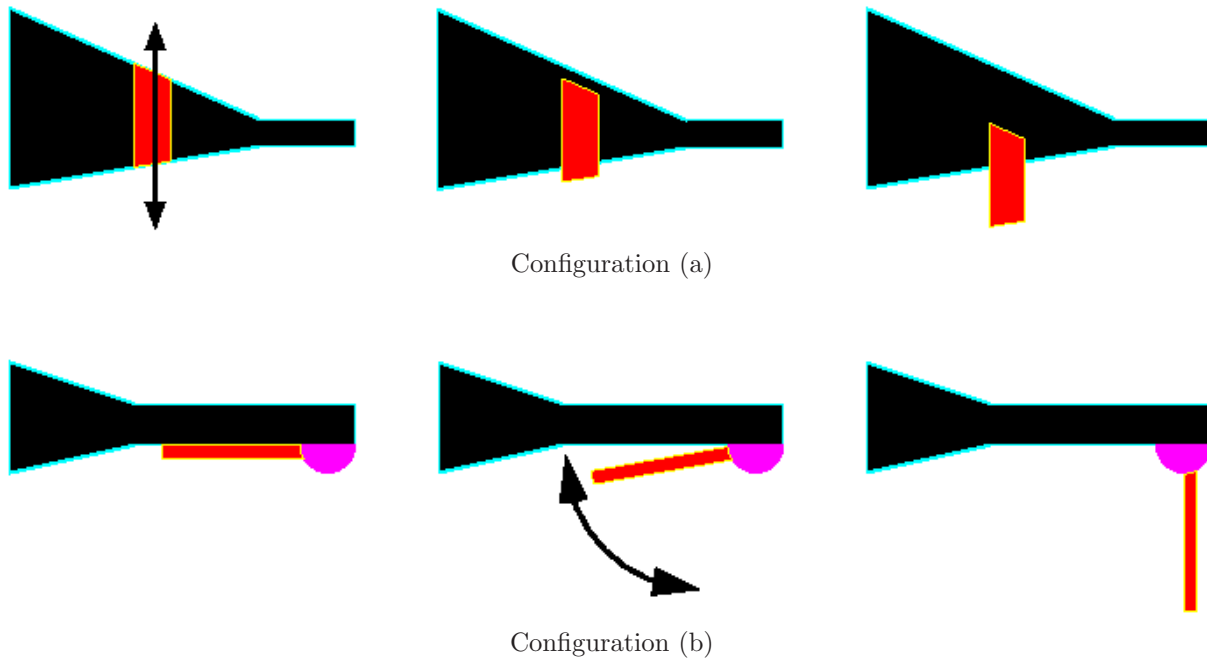
Configuration (b)

Figure 1. Proposed Gurney flap configurations.

(a)   (b)   (c)
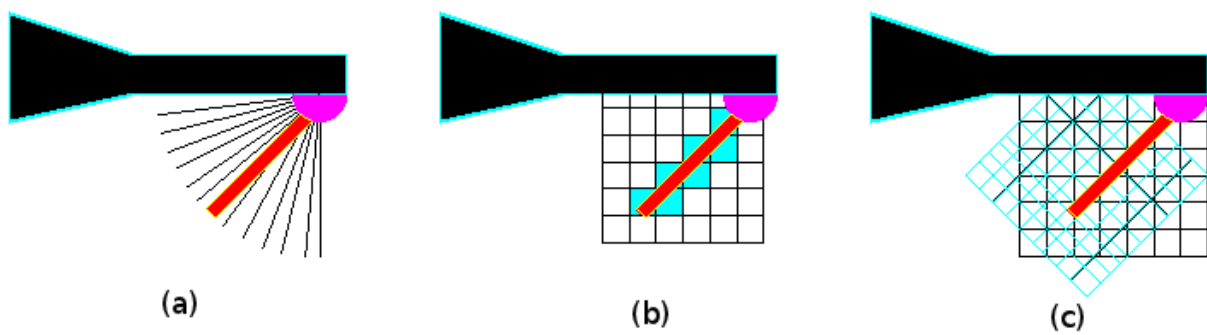
Figure 2. The 3 possible methods for the solution of the active Gurney flap shown for configuration (b) of Figure 1.
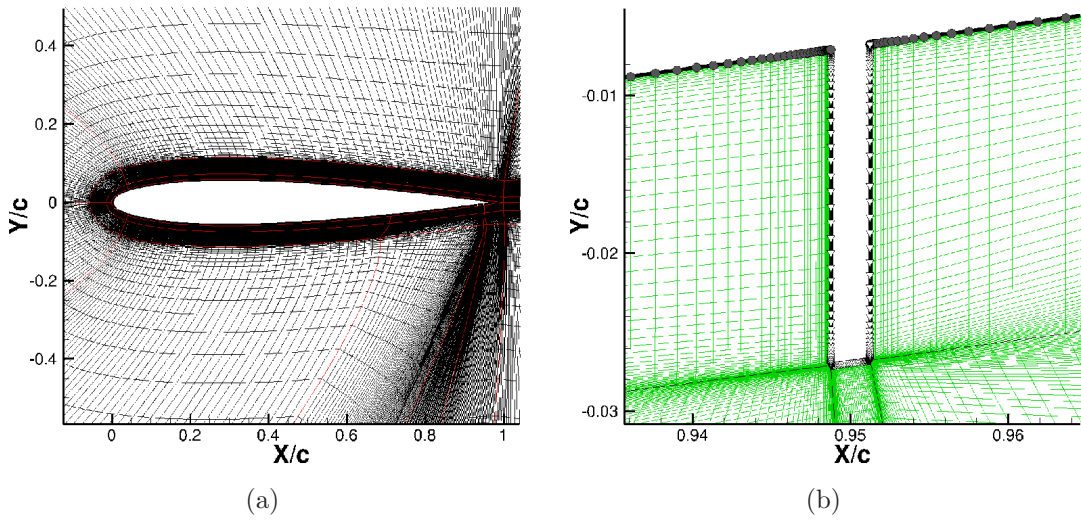
Figure 3. Example of a possible blocking for a Gurney at 95% of the chord. (b) shows a closeup of the Gurney flap. NACA0012 aerofoil, Gurney size = 2% chord, Gurney thickness = 0.25% chord
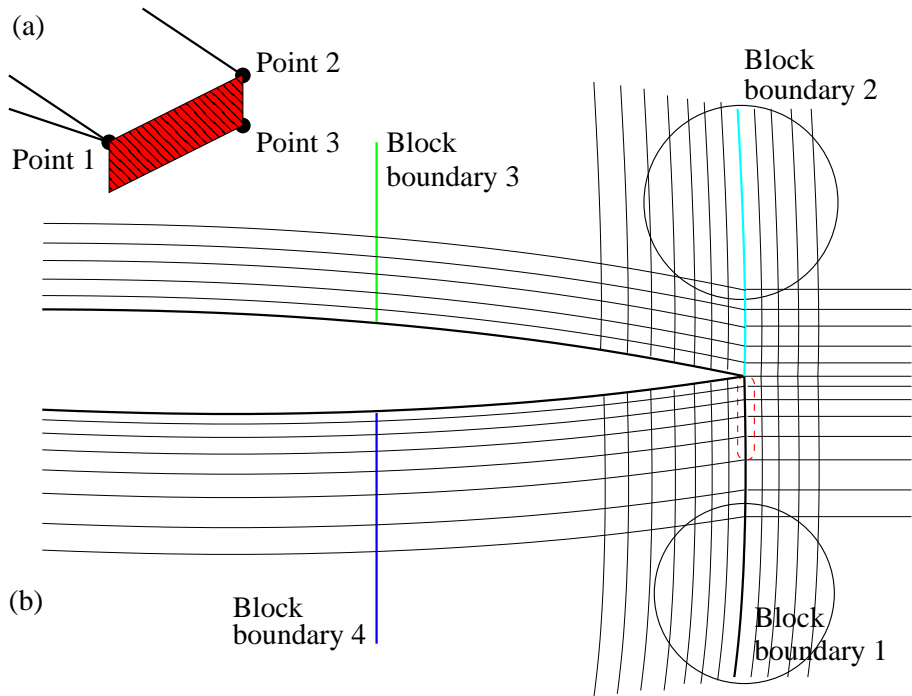
Figure 4. Method for flagging a Gurney flap. (I) Gurney plane definition, and (II) elimination of block boundaries 3 and 4 for not meeting the distance requirements, and part of boundaries 1 and 2 for not meeting the angle requirements. Only the cell faces of the accepted block boundaries which are inside the Gurney plane will be flagged as solid (Gurney flap).
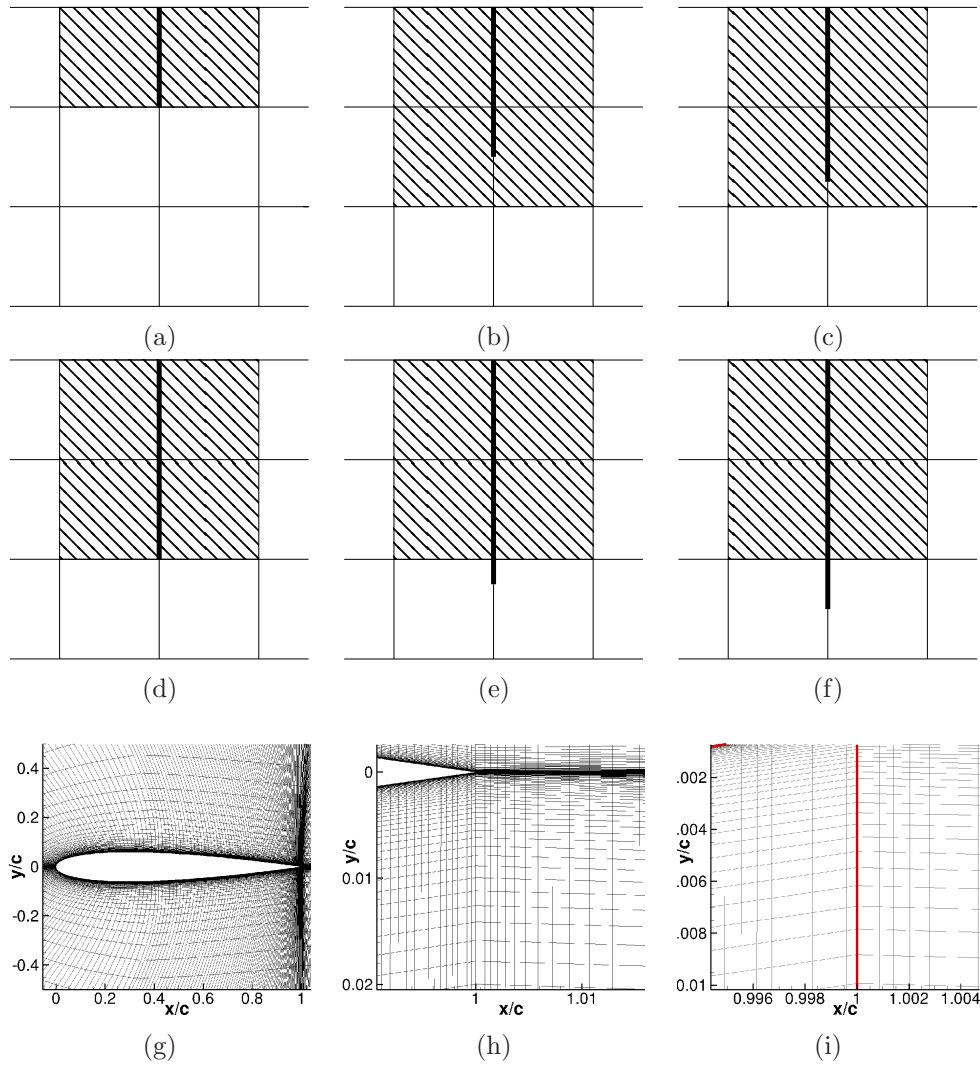
Figure 5. Flagging of the cells - shaded - that require a wall boundary condition applied to their face in order to model the Gurney flap (shown in solid black line). The Gurney flap can change in length without a change in the cells flagged as blocked. Minimal changes are needed in the CFD mesh (g), (h), and the Gurney flap can be seen in (i).
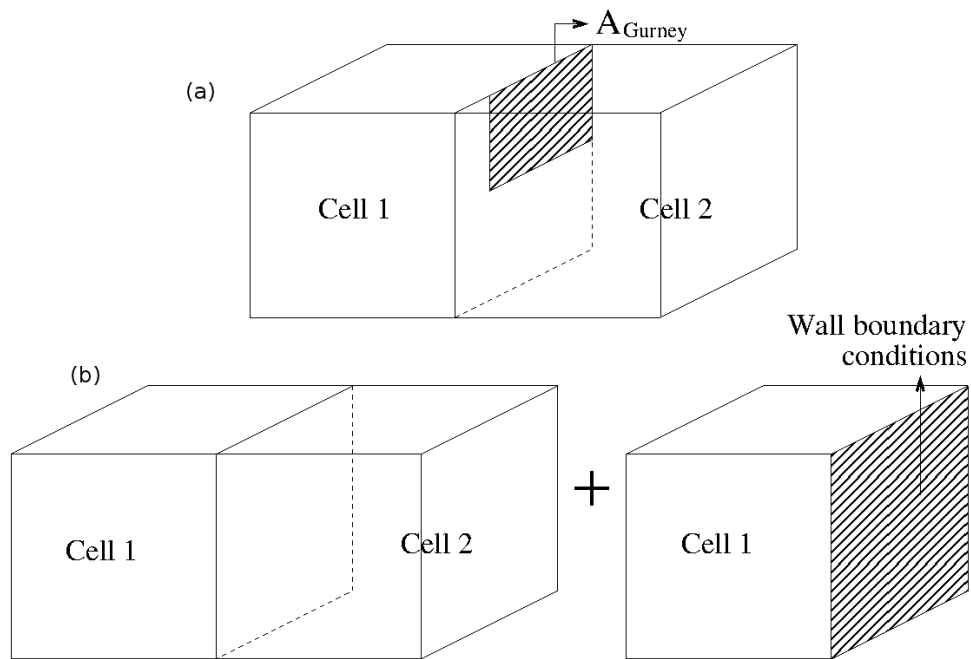
Figure 6. Part-flux method description. (a) a schematic of a Gurney flap covered part of the face between two cells, and (b) calculation of the fluxes twice before weighting them.
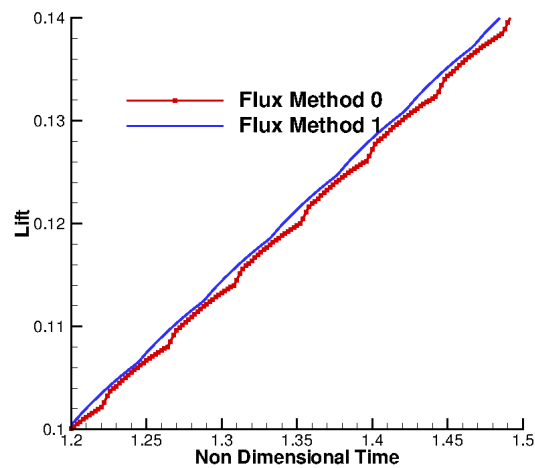
Figure 7. Lift coefficient comparison between the part-flux (method 1) and the full-flux (method 0) methods for a NACA 0012 aerofoil with an actuated 2% chord Gurney flap. $M = 0.2$, $Re = 2.1 \times 10^6$, $\alpha = 0^o$, k-ω SST [32].
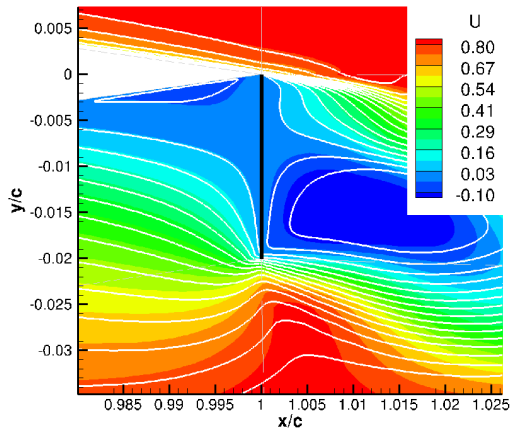
(a) Contours of U-velocity component
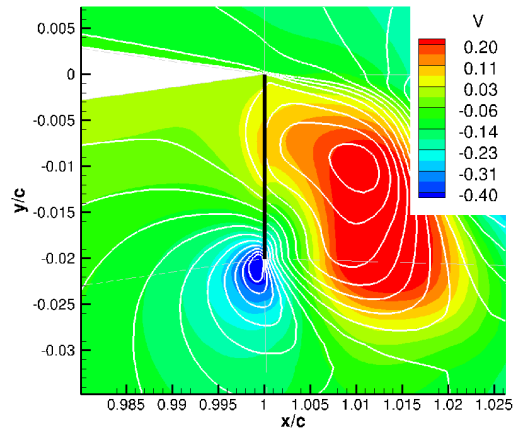
(b) Contours of V-velocity component

Figure 8. Viscous flow around a NACA 0012 aerofoil with an actuated 2% chord Gurney flap. The colour contours represent the solution with the full flux method and the white contours represent the solution with part-fluxes. $M = 0.2$, $Re = 2.1 \mathrm{x} 10^6$, $\alpha = 0^o$, **k-ω SST [32].**
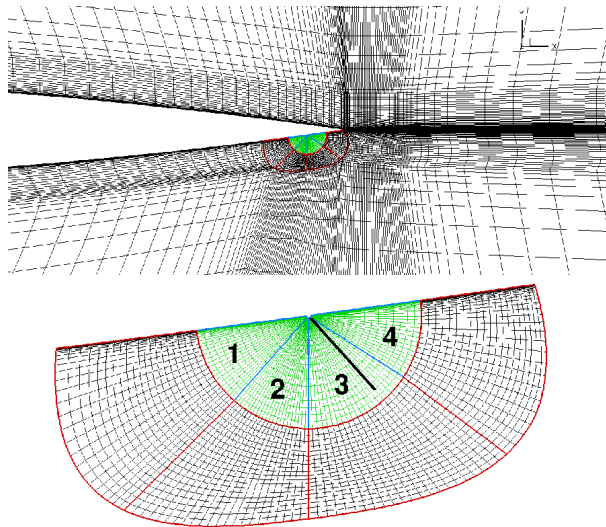
Figure 9. Example of a possible blocking for a Swinging Gurney at 95% **of the chord, and a near view of the topology.**

(a)Definition of the Gurney plane

(b)Flagging cells behind and in front of the Gurney
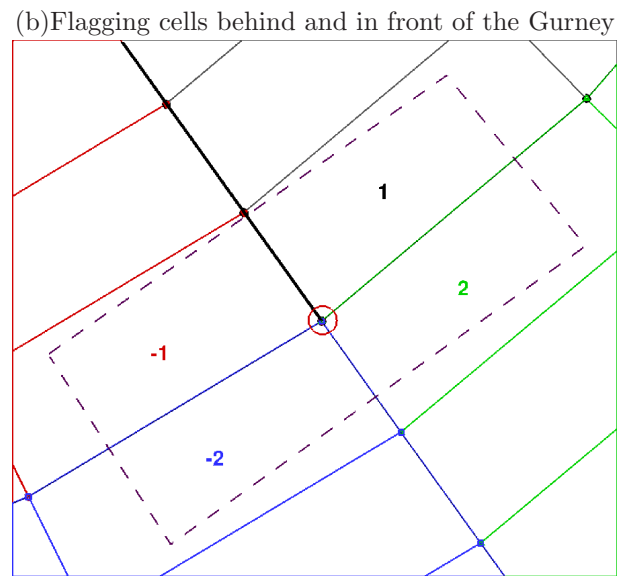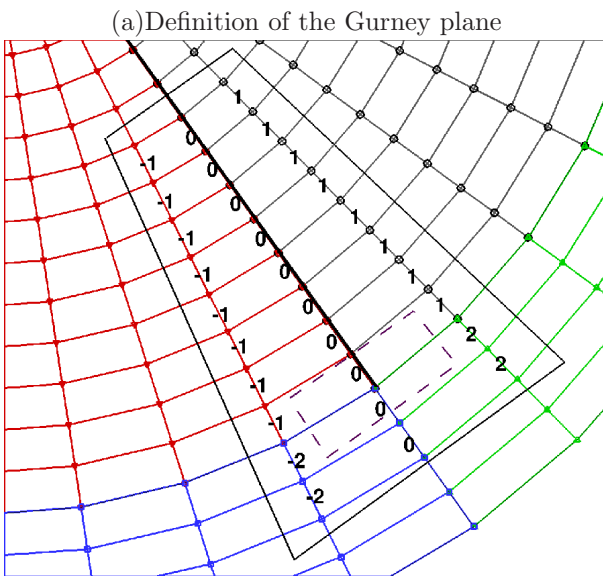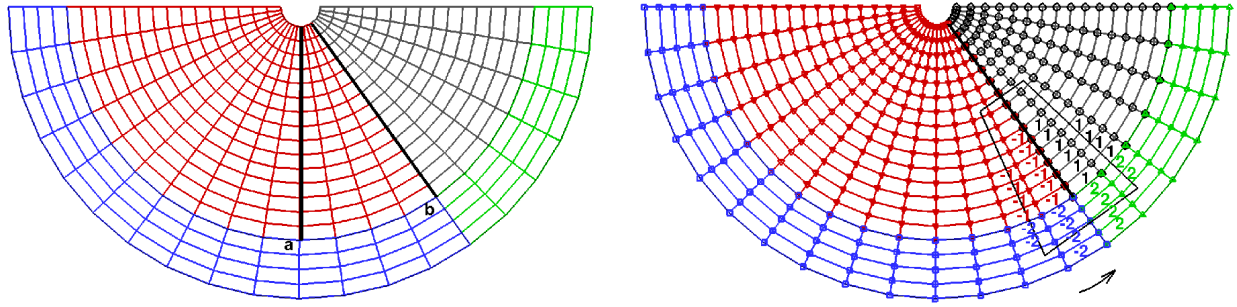
(c)Average the flags on the nodes

(d)Define the end point of the Gurney

Figure 10.   Description of method for flagging wall faces for a swinging Gurney case with HMB2.
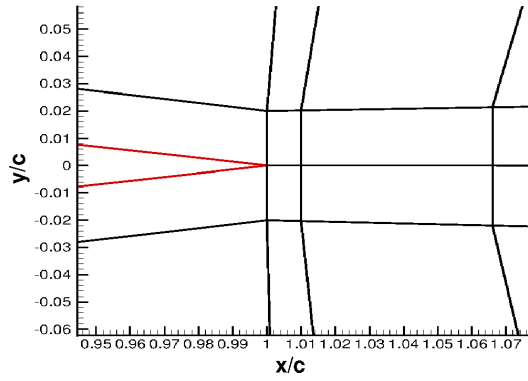
(a) Mesh blocks at trailing edge
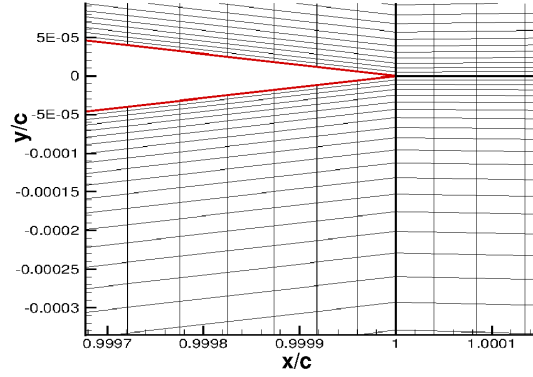
(b) Detailed mesh close to trailing edge
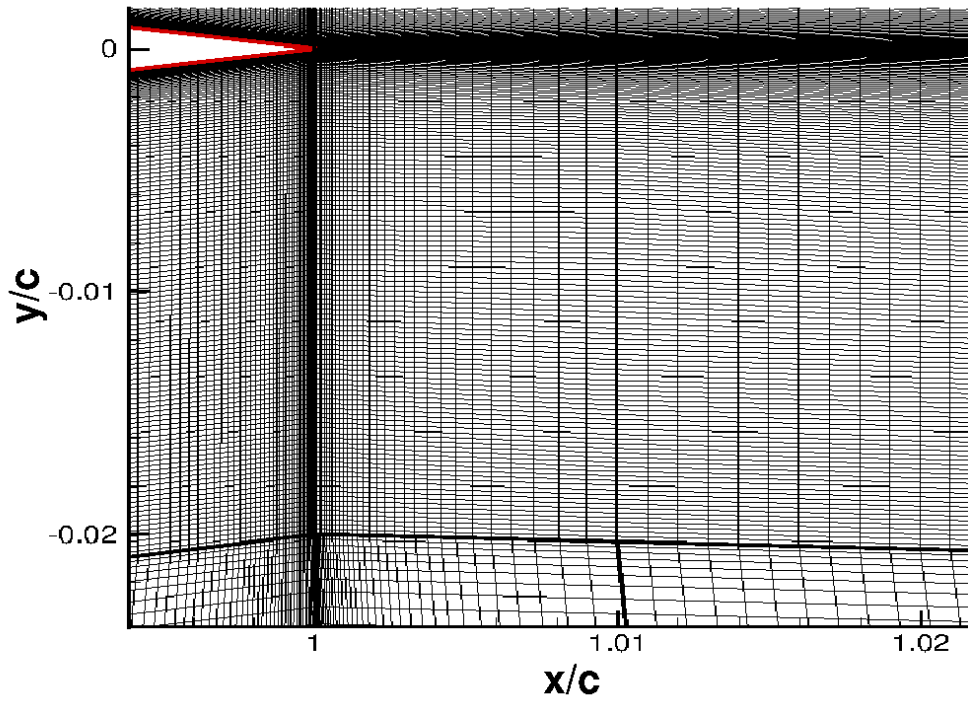
(c) Mesh near trailing edge

Figure 11. Blocking and mesh spacings for a Gurney at the trailing edge.
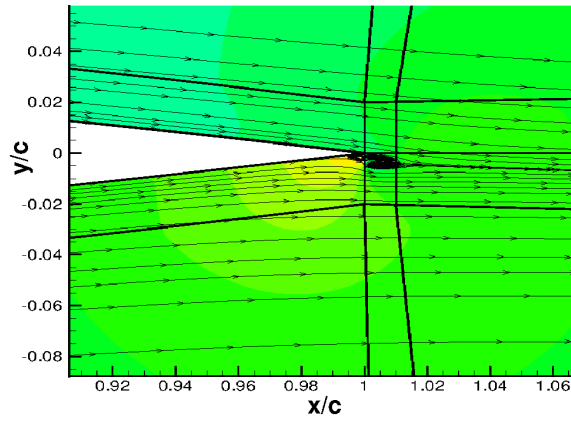
(a) $h = 0.5\%$
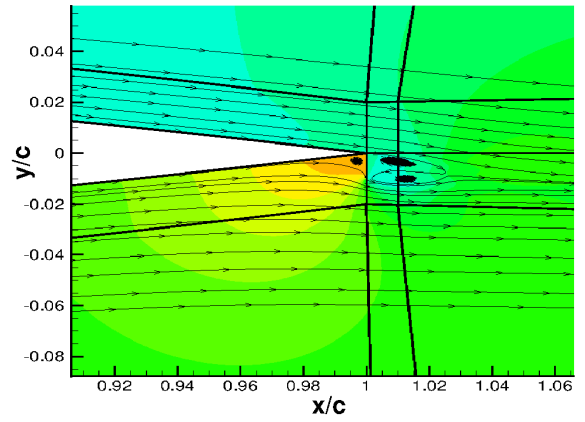
(b) $h = 1.0\%$
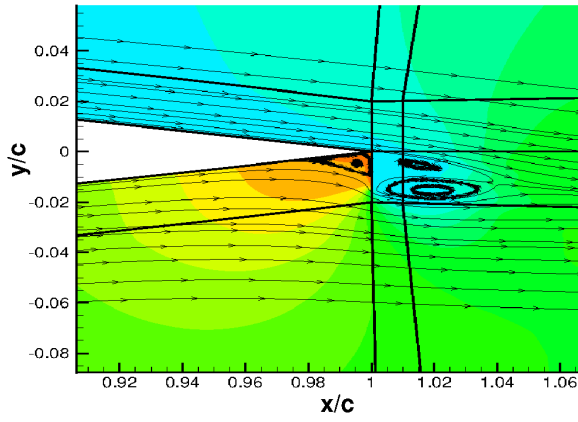
(c) $h = 1.5\%$
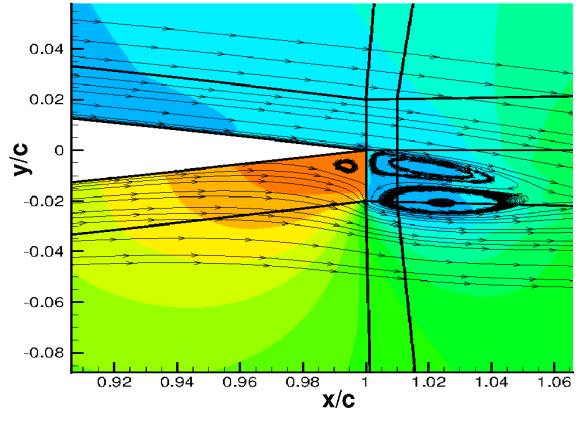
(d) $h = 2.0\%$

Figure 12. The Pressure contours and streamlines for four different heights of Gurneys. NACA0012, $M = 0.2$, $\alpha = 0^o$, $Re = 2.1\text{x}10^6$, k-ω SST [32].

View 1

View 2

View 3

View 4
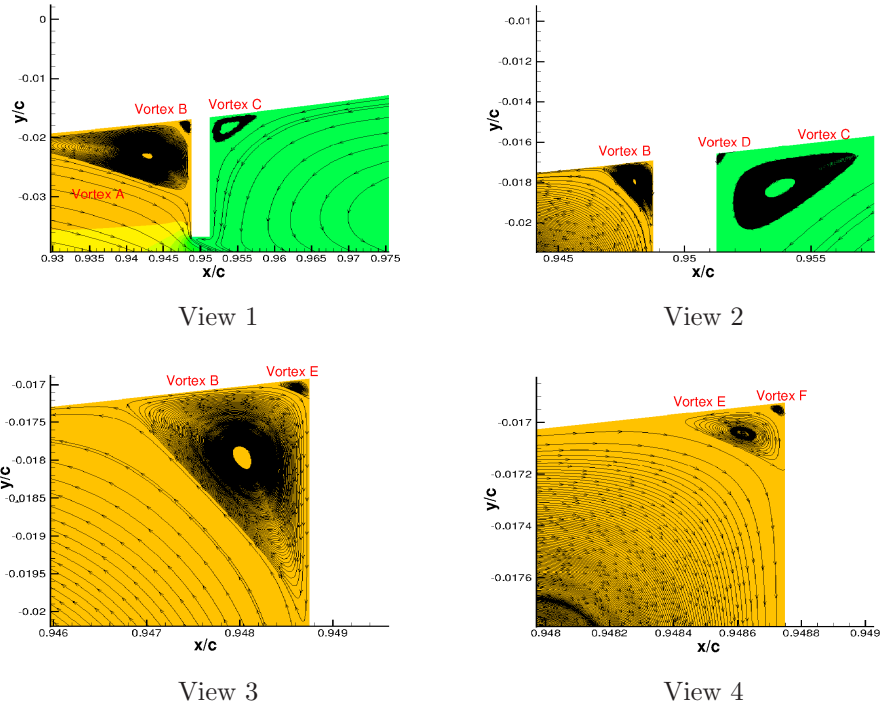
Figure 13. Successive views of the flow near the aerofoil Gurney junction. Streamlines and contours of Pressure coefficient are shown.

C_P and Streamlines

Turbulent Reynolds Number
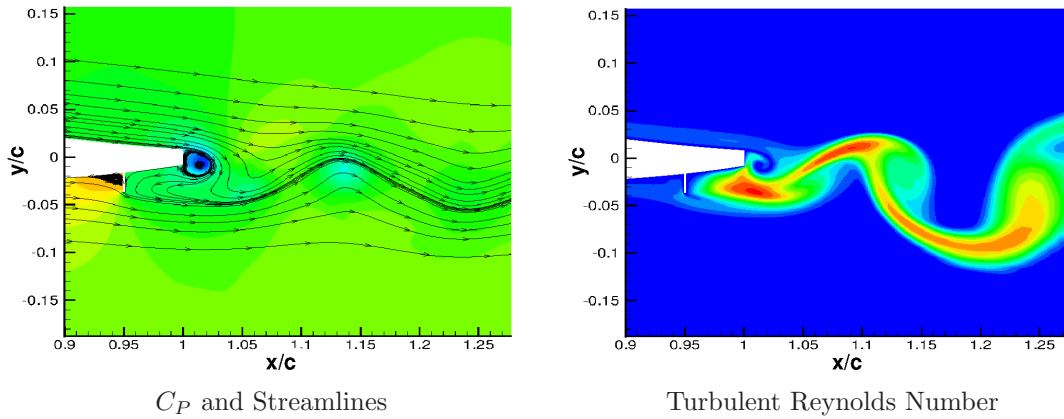
Figure 14. Flow visualisation behind an aerofoil, computed unsteady with a fixed, resolved Gurney and wake. $M = 0.2$, $Re = 2.1\text{x}10^6$, $\alpha = 0^o$, k-ω SST [32].
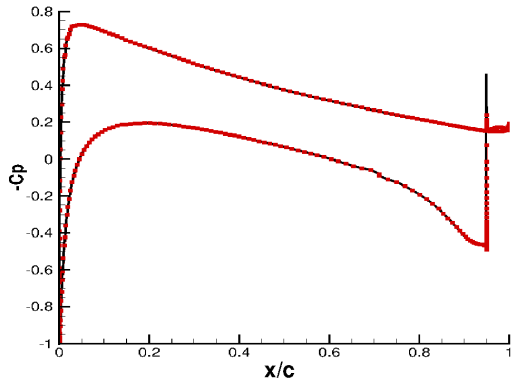
(a) Surface pressure coefficient distribution
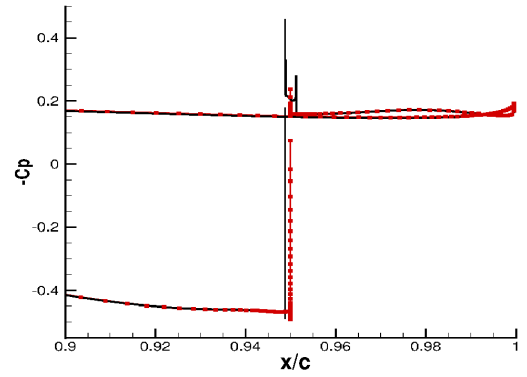
(b) Zoomed view of the surface pressure coefficient distribution near the trailing edge and Gurney

Figure 15. Comparison between thick and thin Gurneys for a NACA0012 aerofoil with a Gurney of 2%c length computed at Mach number of 0.2 and zero incidence angle. Viscous computations were necessary for this case. Dotted line represents the case with the infinitely thin Gurney flap.
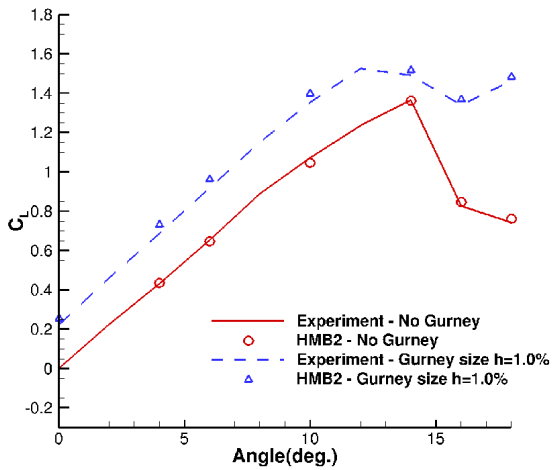
(a) Total Lift
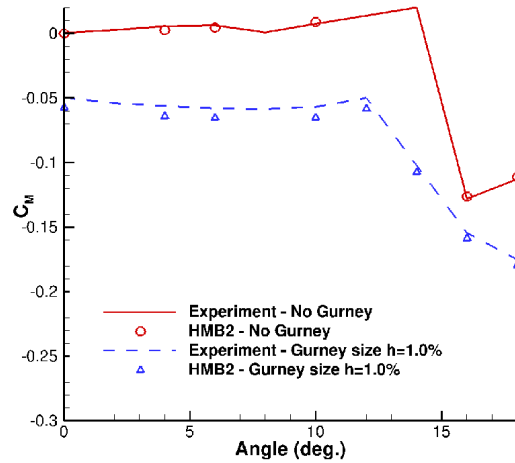
(b) Total Moment

Figure 16. Comparison of loads for different Gurney heights at the trailing edge against experimental data [1, 17].

(a) Angle of attack zero degrees   (b) Angle of attack six degrees   (c) Angle of attack ten degrees
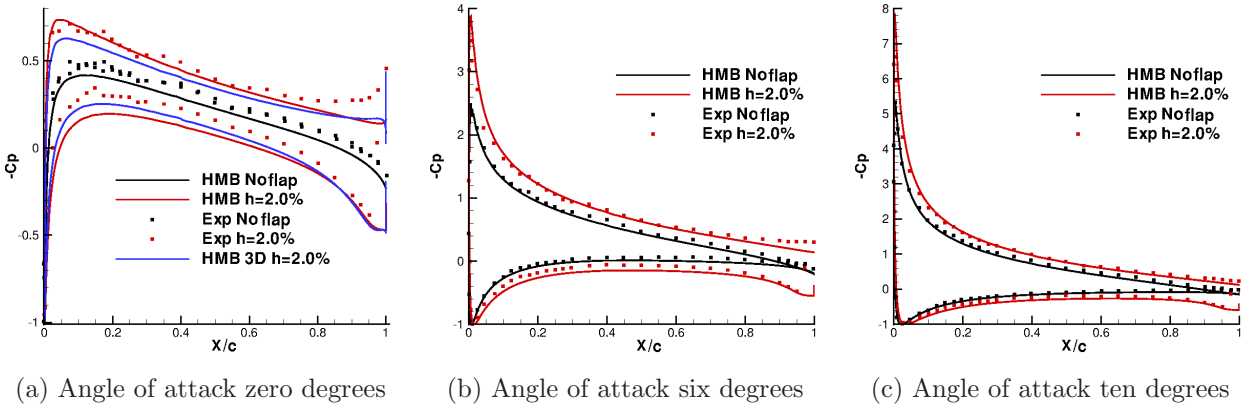
Figure 17. Comparison of pressure distribution of a 2% Gurney at the trailing edge for different angles of attack [1, 17].
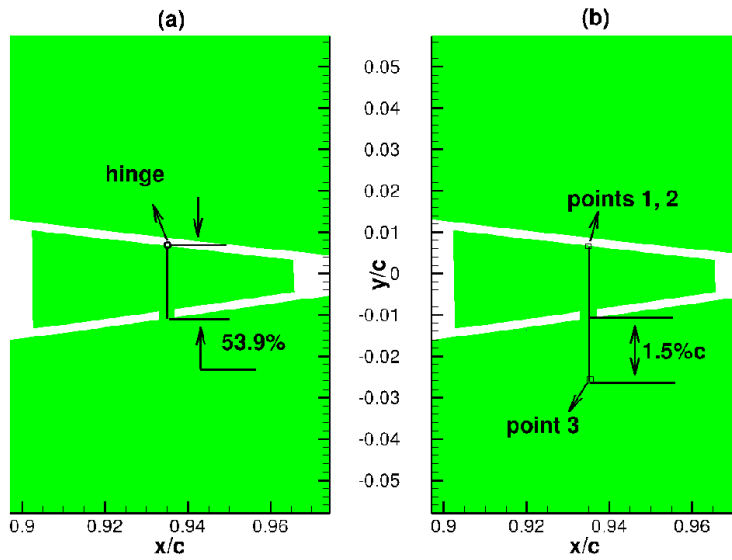
Figure 18. Definition of the actuation of the virtual Gurney used for NACA23012M aerofoil with cavity.

(a)   (b)   (c)
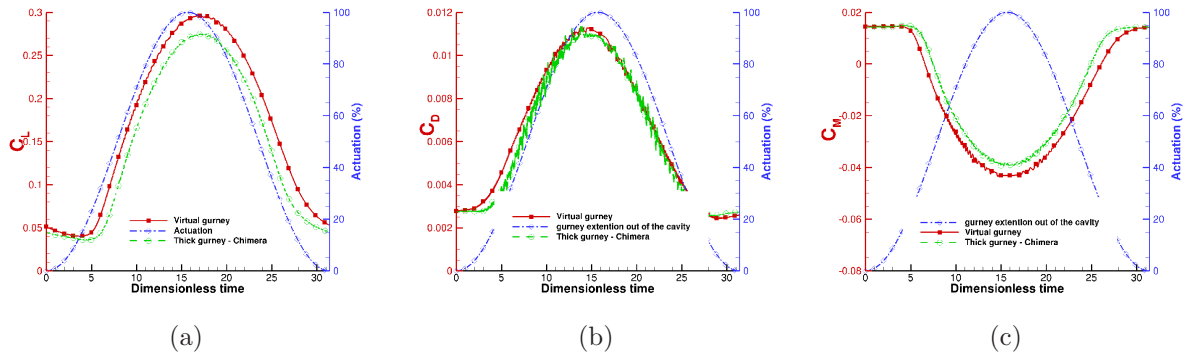
Figure 19. (a) Lift, (b) drag, and (c) moment coefficients comparison on NACA23012M aerofoil with cavity and a linearly actuated virtual and thick Gurney flap of 1.5%c at 93.5%c, M=0.2, $Re = 0.5 \cdot 10^6$.

(a)   (b)
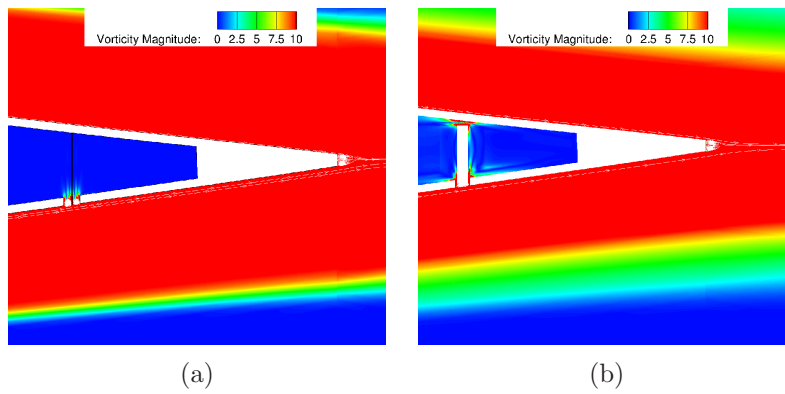
Figure 20. Vorticity magnitude visualization for a NACA23012M aerofoil with cavity and a linearly actuated virtual (a) and thick (b) Gurney flap of 1.5%c at 93.5%c, M=0.2, $Re = 0.5 \cdot 10^6$. The Gurney flap is fully retracted.

(a)   (b)
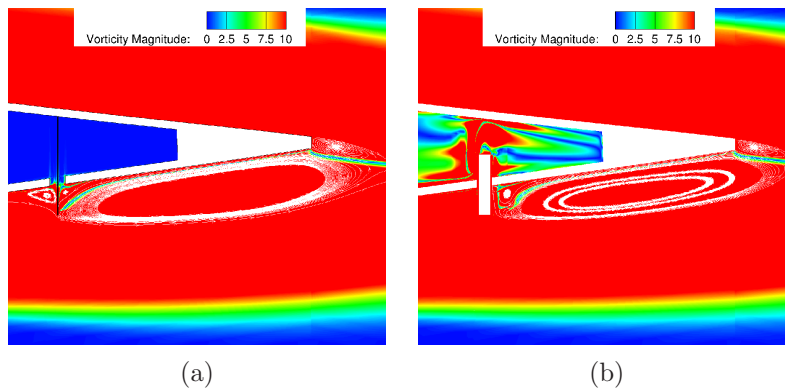
Figure 21. Vorticity magnitude visualization for a NACA23012M aerofoil with cavity and a linearly actuated virtual (a) and thick (b) Gurney flap of 1.5%c at 93.5%c, M=0.2, $Re = 0.5 \cdot 10^6$. The Gurney flap is half actuated.
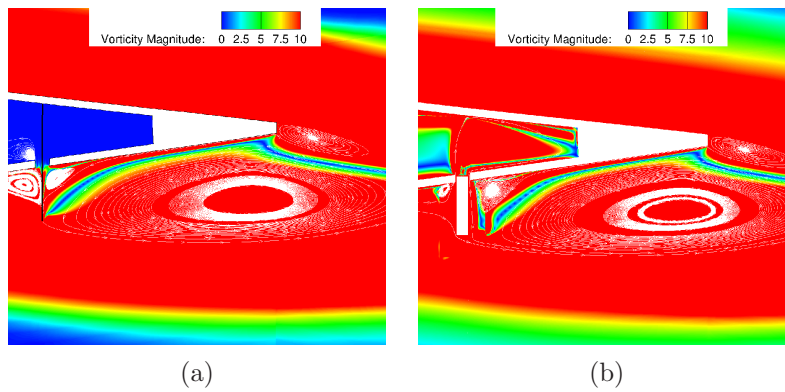
Figure 22. Vorticity magnitude visualization for a NACA23012M aerofoil with cavity and a linearly actuated virtual (a) and thick (b) Gurney flap of 1.5%c at 93.5%c, M=0.2, $Re = 0.5 \cdot 10^6$. The Gurney flap is fully actuated.
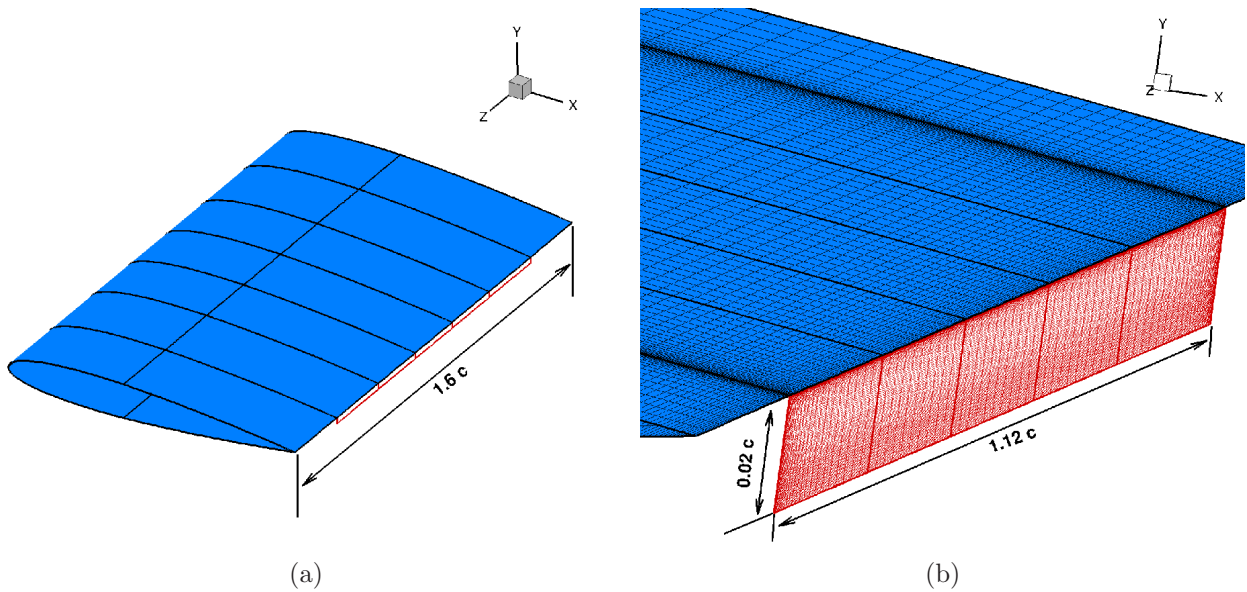
Figure 23. Part-span Gurney flap on a wing. (a) overview and (b) close view of the Gurney flap and the surface mesh.
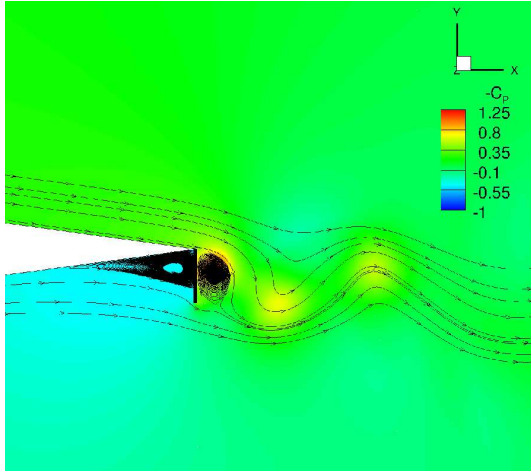
(a) t=1.25
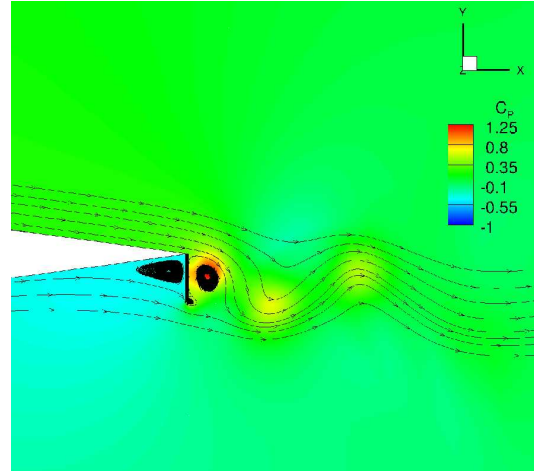
(b) t=3.14
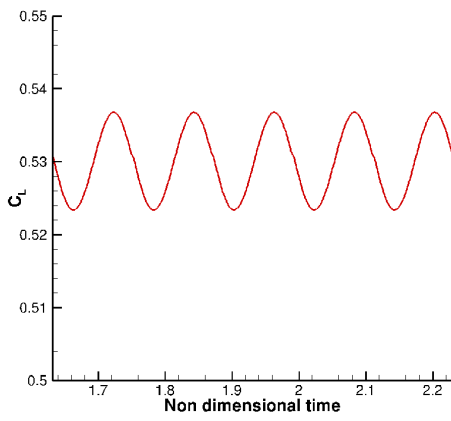
(c) Unsteady case, fixed Gurney
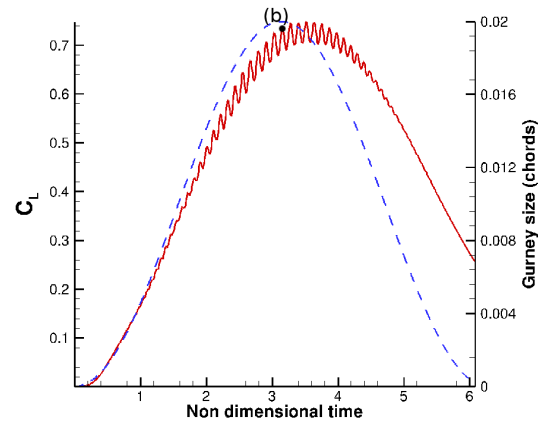
(d) Unsteady case, actuated Gurney
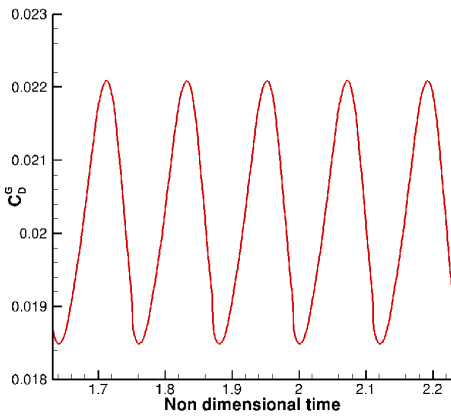
(e) Unsteady case, fixed Gurney
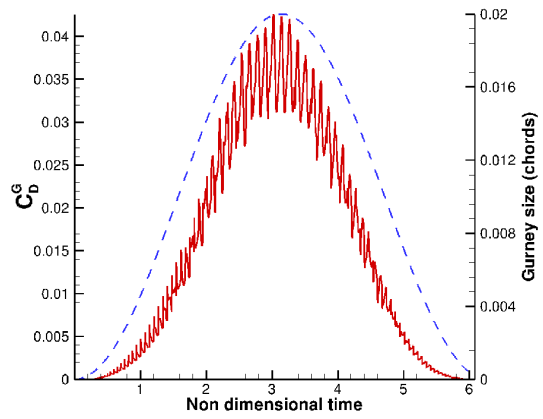
(f) Unsteady case, actuated Gurney

Figure 24. Pressure coefficient behind a fixed (a) and an active (b) Gurney flap, and lift and drag coefficients of the 3D wing computed unsteady with the fixed (c, e) and the active (d, f) part-span Gurney flap.

(a)

(b)

(c)

(d)
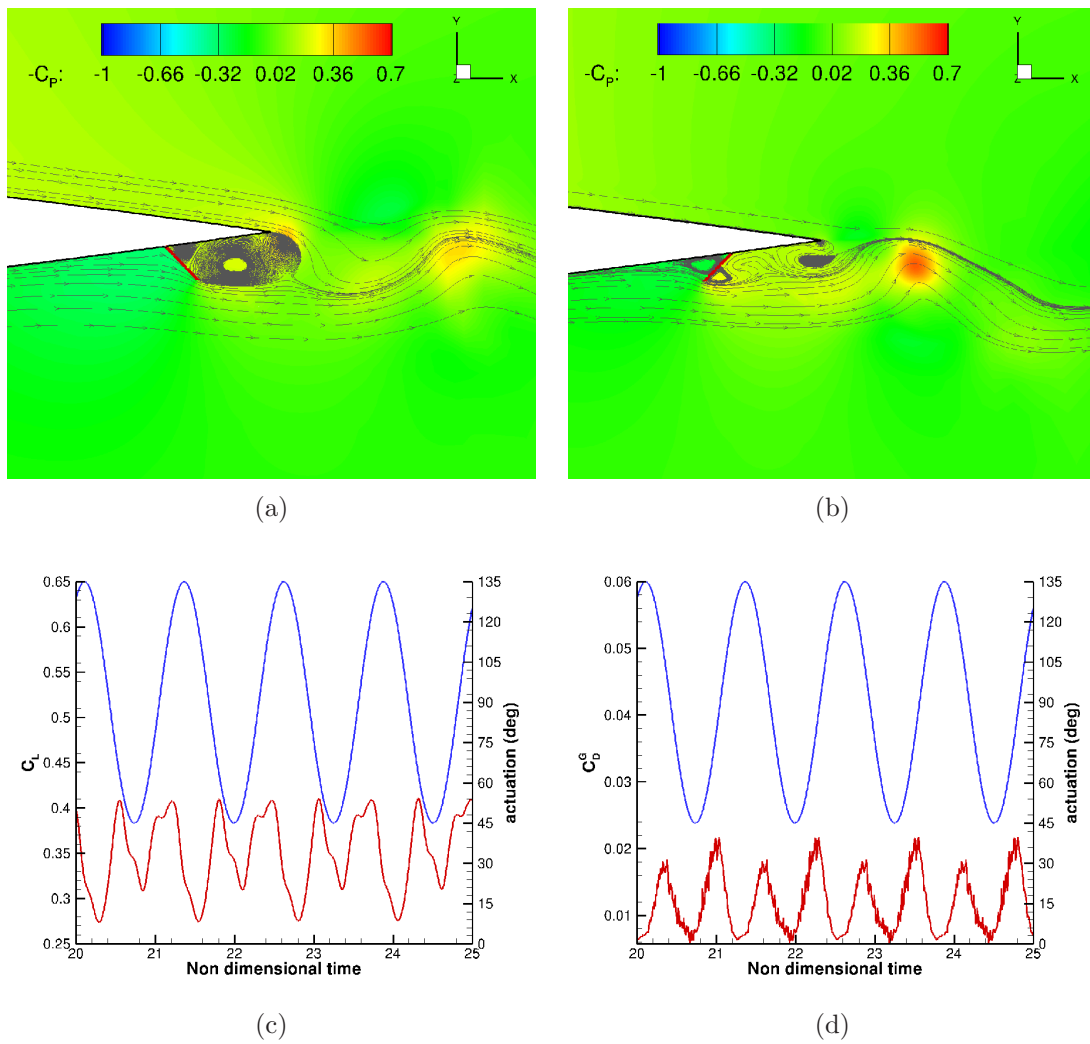
Figure 25. Pressure coefficient behind a swinging Gurney at 45 degrees (a) and at 135 degrees of actuation (b), and Lift and Drag coefficients of the 3D wing computed unsteady with the swinging Gurney (c, d).
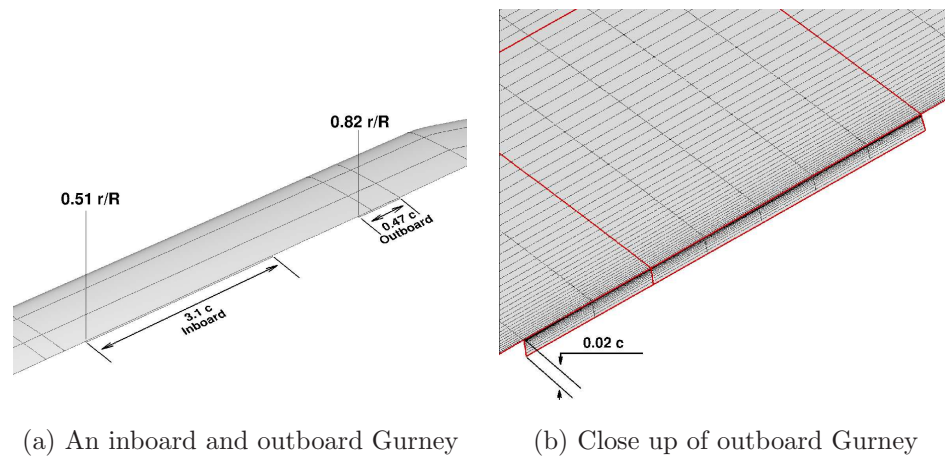
(a) An inboard and outboard Gurney

(b) Close up of outboard Gurney

Figure 26. Visualisation of the inboard and outboard Gurneys on the UH60A rotor.

(a) Blades in global frame   (b) Blades in reference frame

(c) The rigid hull blocks   (d) Blades Surfaces
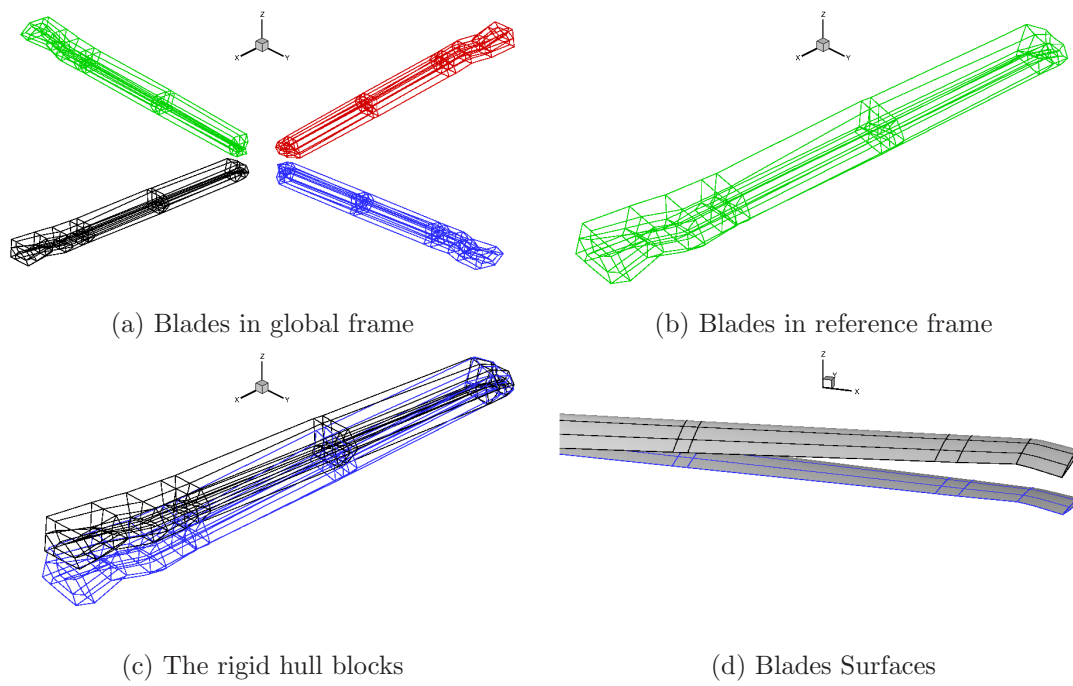
Figure 27. Visualisation of the 4 Bladed UH60A rotor in (a) global coordinates and (b) reference frame. (c), (d) Visualisation of the blade at Azimuth $= 0^o$ in global coordinates (Black) and reference frame (Blue).

(a)

(b)
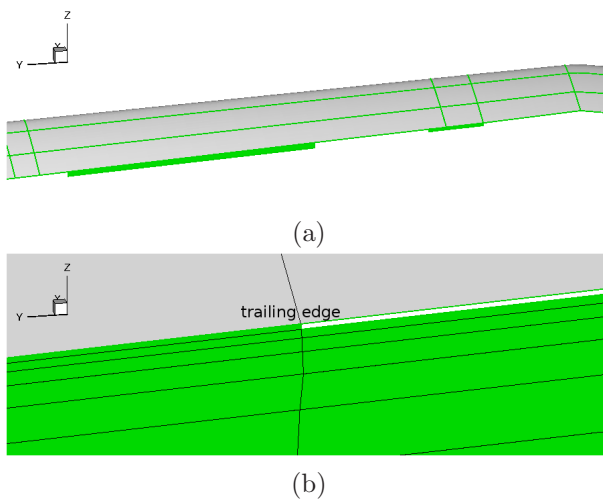
Figure 28. Visualisation of the UH60A Blade in global coordinates for (a) Gurney flaps identification, and (b) a near view for inspection of existing holes.
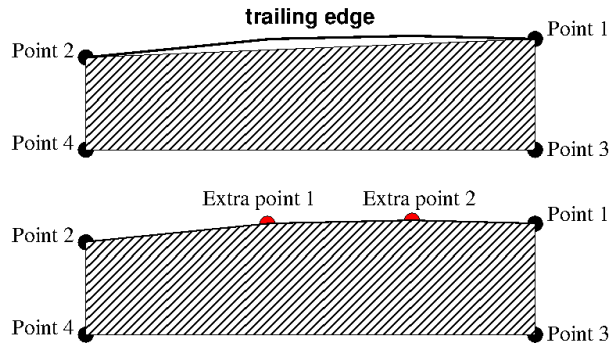
Figure 29. Representation of the Gurney flap from a quadrilateral to an n-sided polygon.
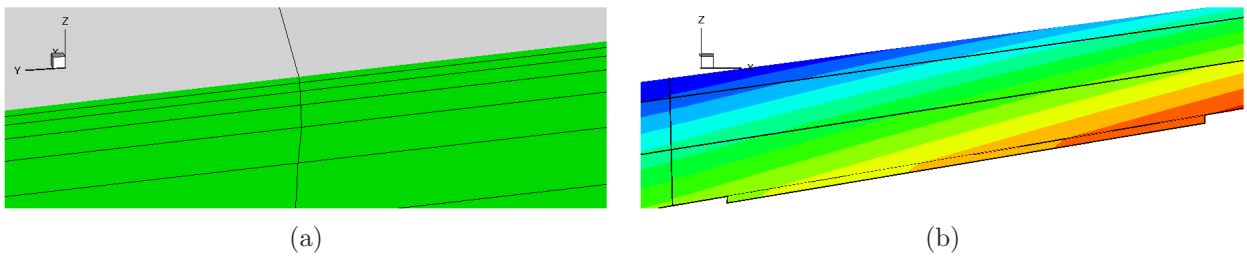
Figure 30. (a) Visualisation of the UH60A Blade in global coordinates and close in inspection of where the hole was, and (b) the z component of the velocity on the blade and the Gurney flap of the UH60A Blade.
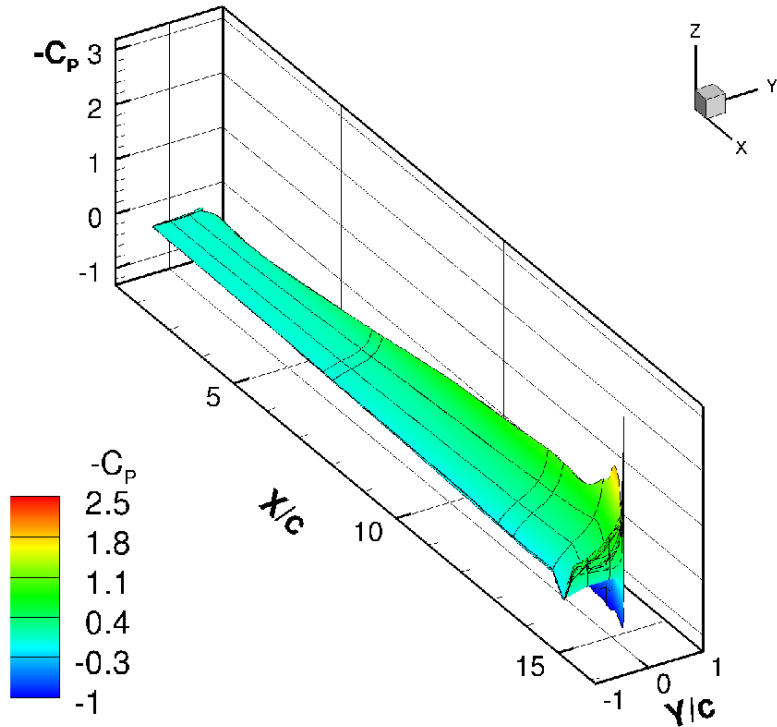
(a) No Gurney flap
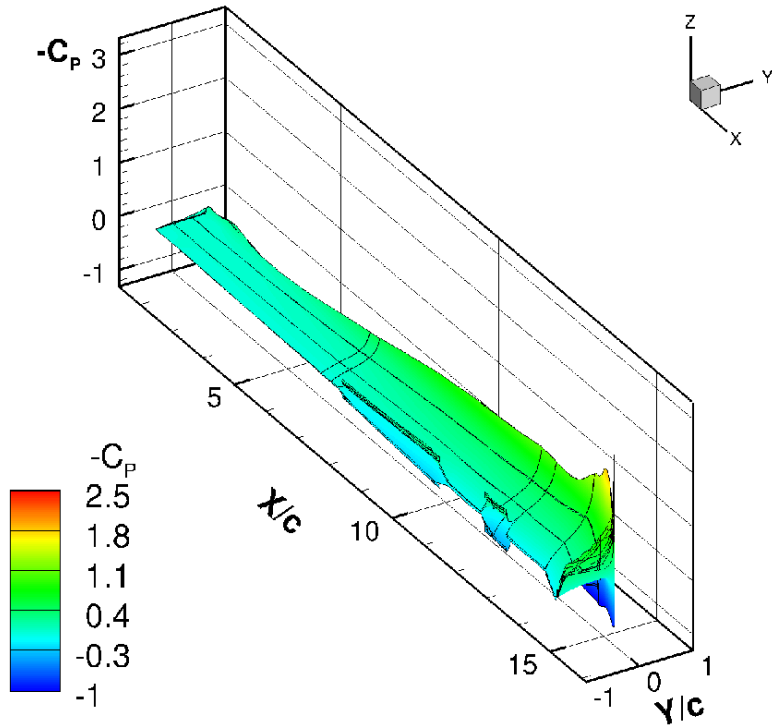
(b) With two Gurney flaps

Figure 31. Surface pressure distribution on the UH60A hovering rotor with and without Gurney flaps. $M_{tip} = 0.63$, $Re = 7.83\text{x}10^6$.
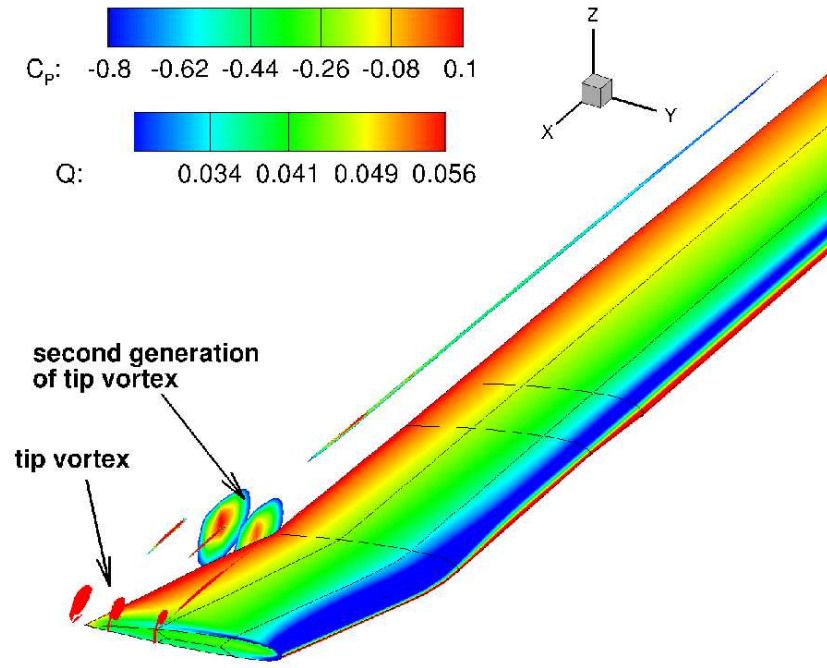
(a) Clean Blade
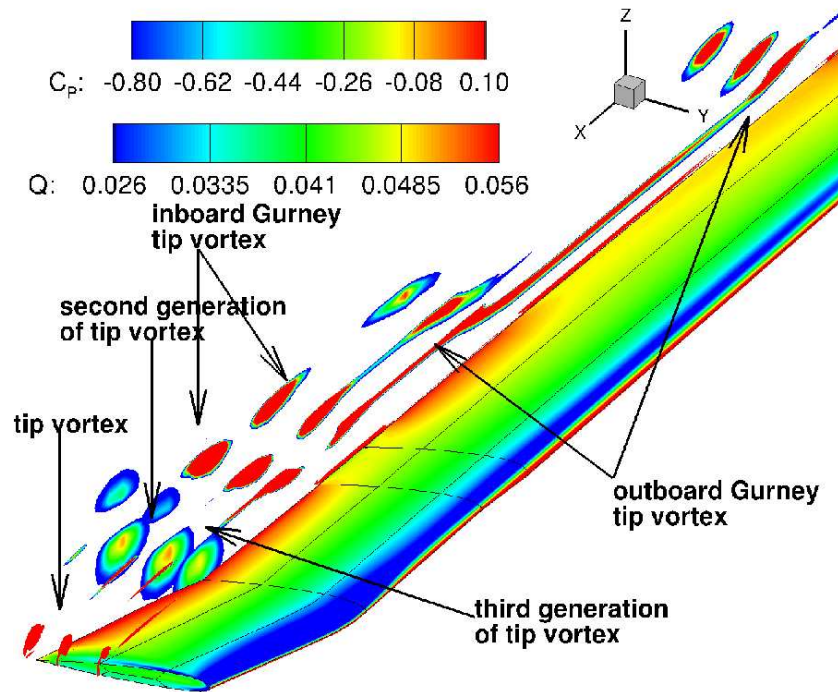
(b) Gurney Flaps

Figure 32. Visualisation of the Gurney effect on the UH60A hovering rotor with contours of pressure coefficient based on the tip speed and iso-lines of vorticity magnitude. $M_{tip} = 0.63$, $Re = 7.83 \times 10^6$.
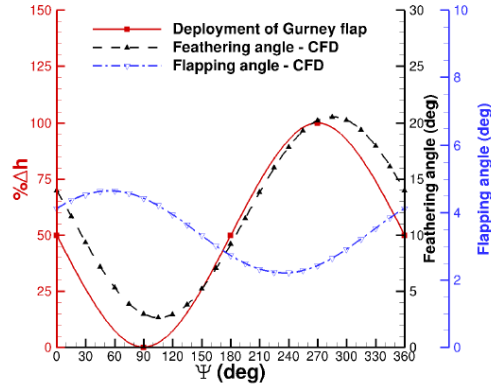
Figure 33. Schedule of pitching, flapping motion, and Gurney flap deployment around azimuth for UH60A in forward flight. 100% deployment represents Gurney size of 2.22% of the chord.
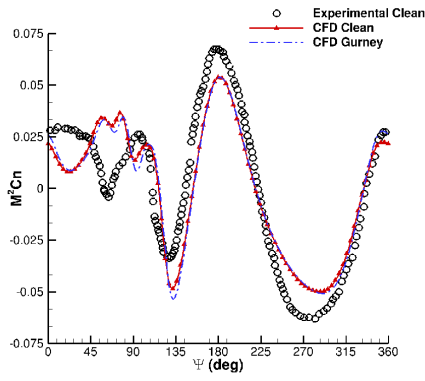
Lift Distribution, no Gurney at section $r/R = 0.675$
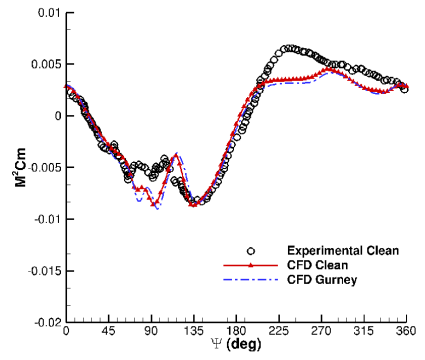
Moment distribution, no Gurney at section $r/R = 0.675$
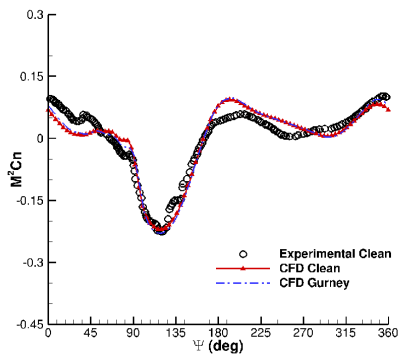
Lift Distribution, Gurney present at section $r/R = 0.865$
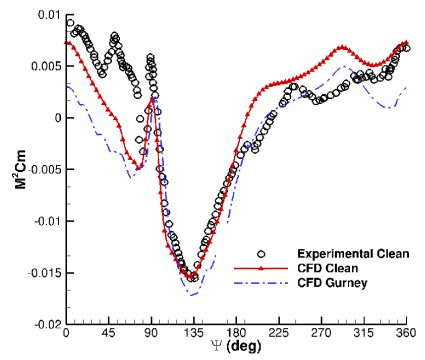
Moment distribution, Gurney present at section $r/R = 0.865$

Figure 34.   Comparison of loads between CFD and Experimental data for UH60-A in forward flight at r/R=0.675 and r/R=0.865.
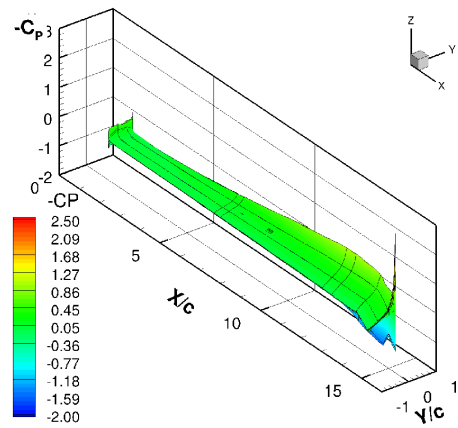
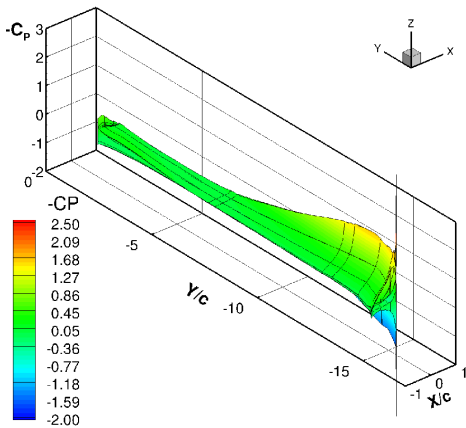(a)

No Gurney 0 deg. azimuth
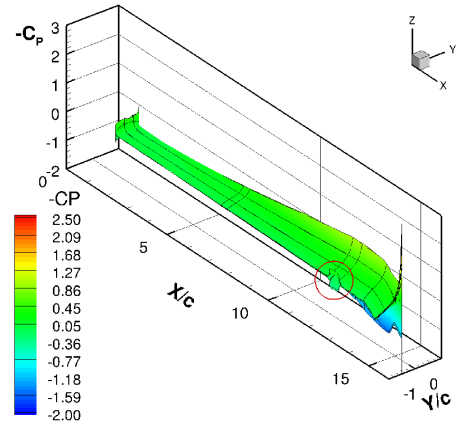
(b)

Active Gurney 0 deg azimuth
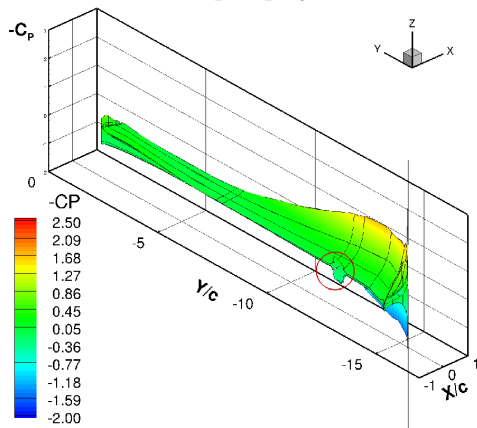
50 % flap deployment
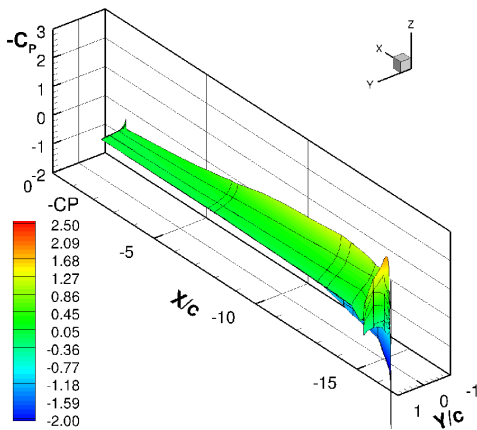
(c)

No Gurney 180 deg. azimuth
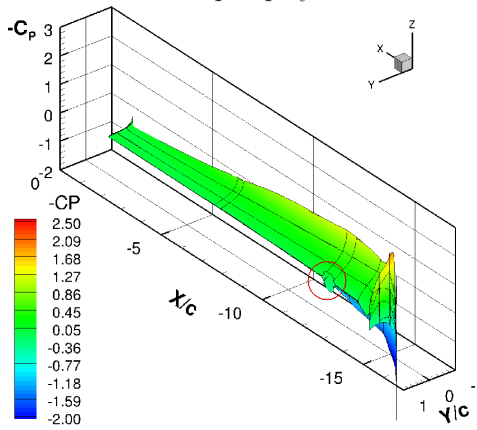
(d)

Active Gurney 180 deg azimuth

50 % flap deployment

(e)

No Gurney 270 deg. azimuth

(f)

Active Gurney 270 deg azimuth

100 % flap deployment

Figure 35. Surface pressure coefficient on the UH60A rotor without and with Gurney flap based on the M_{tip} **of the blade at every azimuthal position.** $M_\infty = 0.2363, Re_\infty = 5x10^6, \mu = 0.368.$
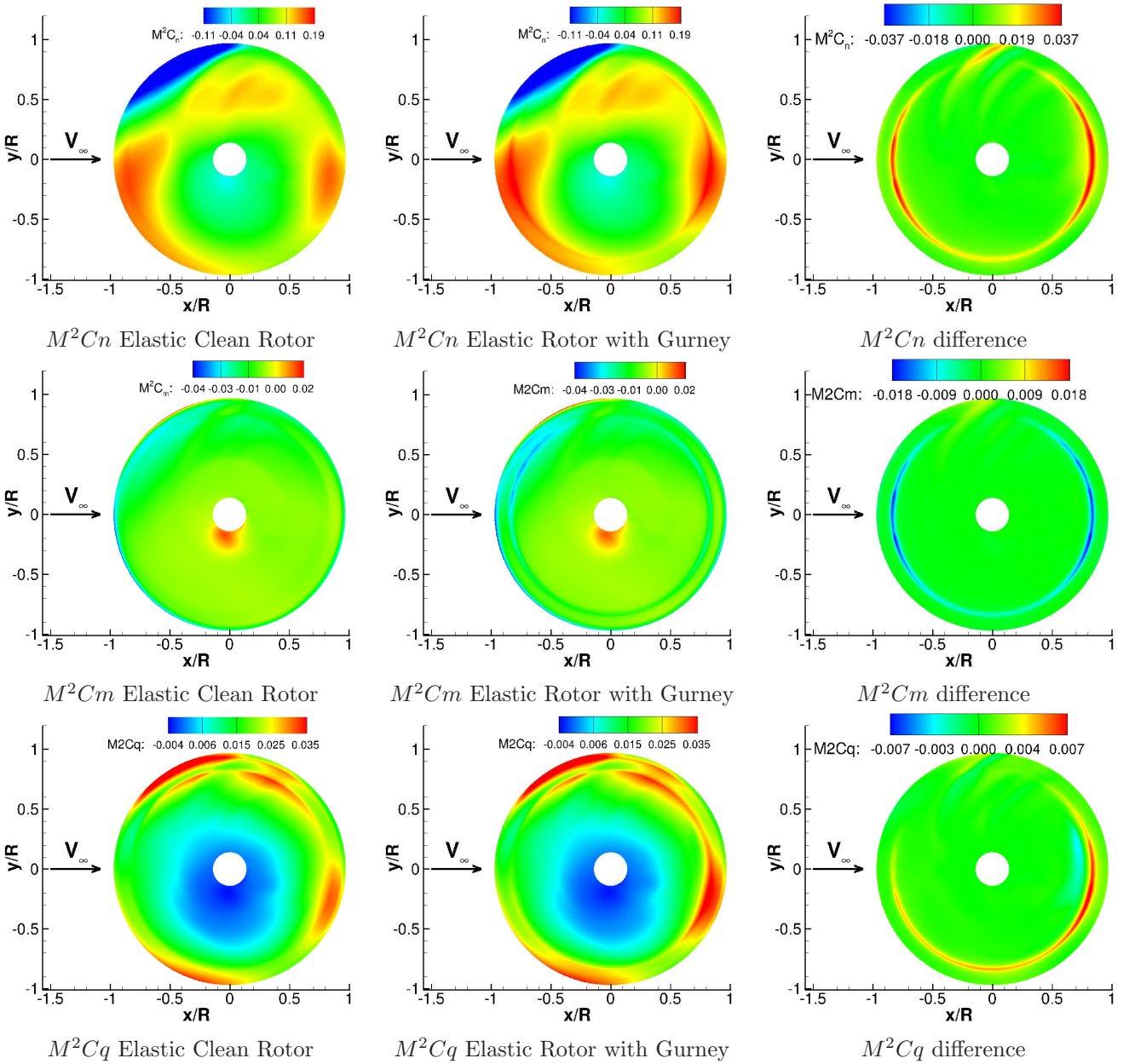
Figure 36. Integrated loads for the UH60A elastic rotor in forward flight with and without active Gurney flap, Coarse mesh.
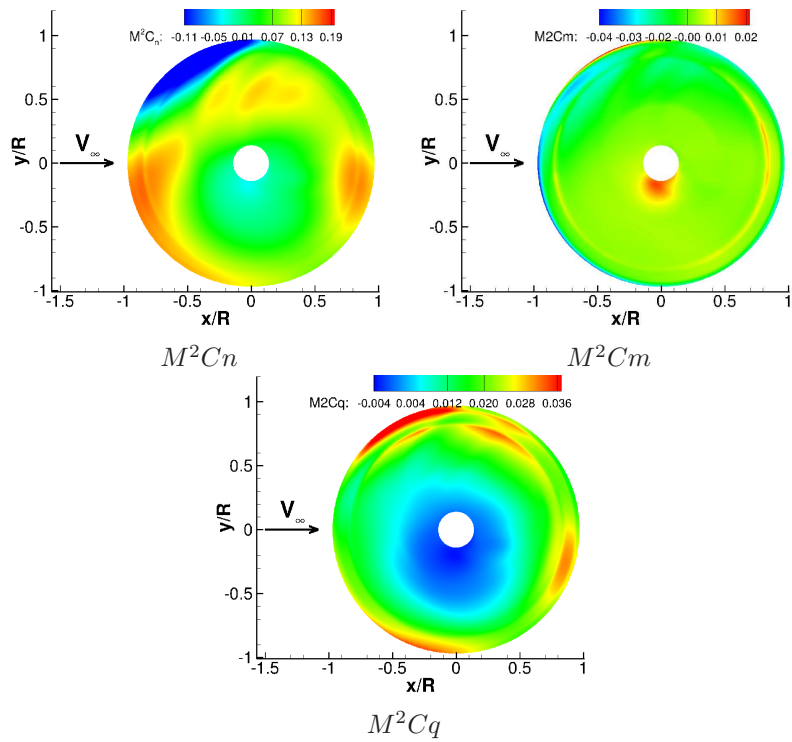
M^2Cn

M^2Cm

M^2Cq

Figure 37. Integrated loads for the UH60A elastic rotor in forward flight with active Gurney flap deployed in opposite direction (towards suction side) - coarse mesh.